UNIVERSITÀ DEGLI STUDI DI SALERNO

Dipartimento di Ingegneria Industriale

Ph.D. Course in Industrial Engineering - XXXIV Cycle

UNCONVENTIONAL INDUSTRIAL MEASUREMENT APPLICATIONS WITH IMAGE PROCESSING

TUTOR
Prof. Paolo Sommella

CANDIDATE
Salvatore Dello Iacono
8800500080

COORDINATOR
Prof. Francesco Donsì

Year 2018–2021

to my family and Fiorita

Contents

List of Figures

List of Tables

Introduction

Nowadays, machine vision systems are widely used in different applications, starting from the automotive field to the entertainment field and the medical applications, Vision Systems play an increasingly important and central role in industry and more. They supplant the human being and support him in carrying out repetitive activities or those activities for which the request for attention or sensitivity on the part of man is not always and constantly assured. The vision systems have undergone a remarkable evolution thanks not only to the technological increase, research and the decrease of the components' cost, both sensors and elaboration systems but above all, thanks to the continuous request of better performances in the existing applications or innovative uses.

In recent years, digital cameras and 3D scanning devices have developed quickly, allowing to measure also rapidly moving objects, thanks to an increasing acquisition rate. This allowed to dramatically increase the application range of 2D and 3D contactless measurements. Image-based measurements are nowadays fundamental for a number of industrial and scientific purposes, including: objects localization and tracking, human-machine interaction, quality control and more. The advent of Industry 4.0 and IoT paradigms have further encouraged the development and use of machine vision-based technologies for both direct applications of vision systems and indirect applications. The use of machine vision systems for extracting measurements from images is well known and has deep roots and numerous applications. The advantages of this kind of technique compared to direct measurements are countless and evident; for example, the possibility to measure inline the dimensional parameters of a

product without interrupting the production flow beside the speed with which it is possible to extract the desired information. However, the use of machine vision for industrial applications does not stop with the acquisition of direct measurements only. Today there are more and more examples of the use of vision systems for applications for which there are no instruments able to extract the desired information, or the use of such instruments would be too expensive or difficult to apply. It is possible to find examples of this kind of use everywhere: face recognition in crime prevention and security or contexts related to shopping or tourism.

The present work is addressed mainly to the last type of applications where the use of vision systems is an alternative and sometimes unconventional way to fulfill a specific objective. Starting from the first chapter with a roundup of applications of machine vision systems in industry and technology, both in terms of software and hardware, which allows the use of images as a raw source of information, then three different application cases, treated within the doctorate, will be presented. The first application case presented is related to an industrial application in which image processing allows to identify the state of wear of a traditional drilling tool but that in some industrial realities, such as aeronautics, becomes a crucial point for maintaining the quality of production. On the other hand, the second chapter presents the application of vision systems in an area between the industrial and domestic: the "water leakage". The application of a device capable of taking images to the dial of a standard analogue water meter makes this device designed and used by water companies a valuable tool in detecting water leaks at the level of domestic users. The last application case presented is the use of image analysis to determine the color of beer for the growing microbrewery industry where the cost of the equipment has a heavy impact, and the use of low-cost instrumentation but still able to ensure high-performance performance is essential. In this case, image analysis is reduced to analyzing a specific spectrum of visible light captured through a photo diode and using signal analysis.

Chapter 1

Industrial Artificial Vision Systems

Nowadays, Artificial Vision Systems (AVS) are widely used for consumer and industrial applications. Their use spreads across many application fields: automotive industry, medical applications, production line inspection, robot control, guidance systems and entertainment, video production and many others. In this chapter, an introduction to Artificial Vision Systems, focusing on Imaging Systems, is presented. An overview of the most common applications of artificial systems is reported with significant interest to industrial applications with references to scientific literature.

1.1   Images Acquisition Systems

In the computer world there are basically two types of images: raster images and vector images. Raster images are a representation of a two dimensional image as a matrix of square points (pixels) with an associate value; generally they consist of a grid of colored, gray, or black and white pixels. They are produced by drawing programs, photo retouching, scanners, photo CD production stations, view cameras, and digital cameras. The properties of raster images make it possible to obtain very large files that are sensitive to resizing

actions.

Vector images, on the other hand, are constructed in mathematical form, that is, with lines, ellipses, rectangles, curves and more complex paths, encoded as mathematical formulas. Their well-organized structure minimizes the size of files and allows you to resize them without losing quality. Vector images can be generated by drawing programs, CAD, 3D and path generation programs can generate vector images.

Creative people and computer graphics enthusiasts tend to define "image" as anything visual element, from the graphical user interface of a program to digital photos and to a file created with a vector drawing program. The use of digital images includes print, video, multimedia, corporate communication (fax, e-mail), electronic text recognition (OCR) and document archiving. Each type of end use requires specific scanning techniques.

As an example, printing includes a wide range of equipment, black and white laser printers, color printers and copiers, photo-units, gravure and sheetfed presses single sheet. The field therefore includes a wide range of documents, from letters to forms, advertising material, newspapers, books, posters and art reproductions. The output requirements for digital images depend essentially on the type of document and the printing equipment. When acquiring an image for printing, particular attention should be used to some parameters like: original document dimension and final image size, scanning resolution, output resolution, output resolution based on the printer size; color field and more.

Another example of the use of images in computers, both for consumer and industrial applications, is the video production. The reproducible color gamut and resolution of a screen or television differs from that of a computer monitor. The resolution and number of colors also differs from one country to another. In this context the variables to consider when acquiring an image are different: output television resolution and update rate, color gamma and video standard as an example.

Human activities make use of image processing in diverse spectrum, in [TA05] several examples are reported:

- **Visual Inspection** used in industrial environment to improve the productivity and the quality of the final product in manufacturing; an example of how old this method is its use in automatic inspection of incandescent lamp filaments installed by General Electric Corporation where the silhouette of the incandescent filament is generated from a binary image and then analyzed to identify the non-uniformity in the pitch of the filament geometry inside the bulb. Faulty component identification is another application field for automatic visual inspection (AVI) and more often makes use of infra-red images to identify faulty components in an assembly.

- **Biomedical Imaging**, various examples of imaging produce different biomedical images that necessitate of different imaging processing for the purpose of medical diagnosis [JL17, Sue09] like X-ray, computer aided tomographic (CT), images ultrasound, MRI and others. Some applications of biomedical imaging are quantitative measurements such heart size and shape for *heart disease identification*, image analysis can be employed to radio-graphic images to classify heart disease. Another important application is the *lung disease identification*, it uses chest X-ray images to identity solid tissues: structures containing air appear as dark while solid tissues, like bones, appear lighter depending on their softness. Segmentation of anatomical structures in ultrasound images remains an important step in computer-aided diagnostics [YT19] and therapy in skin lesions. One example is atopic dermatitis in children which requires an objective and non-invasive method to examine the skin condition before and during the therapy [PG21, Mes21].

- **Defense surveillance** is another field of application of image processing techniques and an important area of study. There is the need of

continuous monitoring of the land and oceans using both aerial and terral surveillance techniques in order to recognize and localize objects, like vehicles or humans, in remote part of the land or of the ocean. The objective is not only recognize the position and the distribution but also the moving direction (in the eight possible directions) of these objects. The applications are both military and civil, like search and rescue: the search for survivors in collapsed buildings from earthquakes, explosions, or poor building construction is a difficult and dangerous task. Remote visual inspection enables operators to search in cavities through small apertures with minimal debris disturbance. Fire and rescue services use videoscopes to more safely check buildings and to perform searches in accidents where great care is needed in the rescue of survivors. Video surveillance, criminal identification, building access control are other examples where image processing can be applied in order to recognize a person using only few image images [KJFA20].

1.1.1   Industrial Applications of Artificial Vision

Artificial vision systems have been applied in the industrial field for about twenty years, even if the first operations on images go back as far as the mid 1960s and in the following decades have been produced the first studies on vision in the robotics field. Typical applications are automation of existing visual existing visual controls. Early work at a range of institutions, including the National Physical Laboratory (UK), SIRA (UK), SRI, MIT and Edinburgh University, demonstrated the potential of machine vision in inspection, robotic control and automated assembly. Machine vision is an umbrella term used to describe many different types of vision systems, but in general, machine vision systems are used in the automated processing, analysis and understanding of images in an industrial environment [BGB97].

Machine vision inspection systems now appear in every major industrial sector, areas such as electronics, automotive, medical, food, and manufacturing

industries [BW94, BDG94, CH82]. For the majority of machine vision applications the cost of the vision system is small, relative to the total cost (and overall technology content) of automating a new production line. In modem manufacturing the machine vision system is used to inspect a large number of products rapidly while the human inspector can then perform slower but more detailed inspection on objects that the machine vision system considers to be borderline cases.

In [DTP03] a breakdown of artificial vision is reported; the same is replicated in Figure 1.1, the classification is open and several fields overlaps. As can be seen, artificial vision is conceptually divided into machine vision and computer vision. Industrial machine vision contrasts with high-level computer vision, which covers more theoretical aspects of artificial vision, including mimicking human or animal visual capabilities.
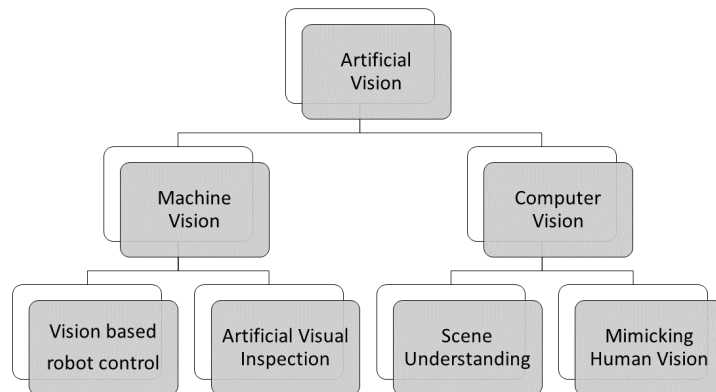
Figure 1.1: A breakdown of artificial and computer vision, from [DTP03].

The vision system can provide an output indication of the product good/scrap, or, in combination with a statistical process analysis, provides also a feedback for the control of the working parameters and detect anomalies before obtaining pieces out of tolerance or however unacceptable by the customer.

Industrial applications of image processing and visual inspection are different and in [CS18] are subdivided in the following categories:

- **Object recognition** or identification: mostly involves reading barcodes and data matrix codes to identify and categorize various products. This is crucial for error-proofing production and packaging processes. Additionally, it is much faster and more accurate than manual error proofing. Machine vision identification can also be used for optimizing productivity by identifying bottlenecks in production pipelines.

- **Positioning** and guidance has numerous useful applications in the manufacturing industry. For the most part, it involves locating a specified part and ensuring proper placement and positioning so that production runs seamlessly and with minimum errors and downtime. Machine vision techniques can also be used to specify the location and orientation of a particular part. The information can then be transmitted to a robot or machine controller for production purposes. Machine vision guidance enables more efficient and more accurate production than manual positioning with employees, especially in assembly lines or arranging parts on pallets where robots are present [Ale83].

- **Completeness check** that mostly involves some kind of object detection. In object detection, the algorithm looks for individual objects rather than the entire image. Here the algorithm is essentially trying to determine objects present or absent in the image as opposed to classifying the entire image. Varieties of techniques are used to perform efficient object detection. Object detection algorithms can be applied at various points within the manufacturing chain such as quality management, inventory management, sorting, assembly line, etc.

- **Shape and dimension check**, also known as *gauging*. In this kind of application, a fixed-mount camera identifies two or more points on an object as it passes by on the production line. If a discrepancy between the distances measured and the distances programmed into the vision system is detected, the part is pushed off the line as it contains some

form of a production error. Machine vision guidance provides greater speed and accuracy over traditional techniques such as contact gauging.

- **Surface inspection** image processing and machine vision is principally used for the flaw and defect detection. Machine vision inspection and flaw detection offer greater flexibility to inspect a wide variety of objects in a large number of industry applications, including decay in agricultural products, flaws in textiles, branding marks in prescription tablets, and more. Inspection done using machine vision is much quicker and far more accurate than manual inspection processes.

In [CD13] also two more areas are added to image processing categories:

- **Color image processing** intended as the evaluation of color information in images for industrial image processing applications. Color images contain more information about the scene captured than gray level images and for this reason they need more memory and computational power to be elaborated but it is necessary for some applications to use color image processing [WGW$^+$95]. The trivial example is the identification of an object color, another typical task is verifying the position or the presence of a specific color object. Generally, human observers cannot discriminate between two colors if they can be described within an isodiscrimination contour; in this case visual inspection can be used to discriminate un-perceptible color differences to human eyes. An example is the automated visual inspection for cotton quality in textile industries [TVTV99, AE15] because it is subject to contamination from numerous sources, like botanic trash, that are difficult to remove and affects the quality of the final tissue increasing the breakability of cotton yarn. There it is necessary to identify foreign matter in the cotton, conventional detection methods have been performed by human workers but automatic visual inspection with high-resolution cameras represent a several advantages and meets the requirement of real time inspection

[ZL14]; in these application both high-speed CCD or CMOS cameras are used in line scan or area scan configurations, the first of which is more flexible and convenient.

- **3D image processing** encompasses the visualization, processing and analysis of 3D image datasets, for example those obtained from a Magnetic Resonance Imaging (MRI) or Computed Tomography (CT) scanner. With 3D image processing, it is possible to model structures of extremely high complexity, for example anatomical structures in the human body, microstructures in a material sample, or defect-ridden industrial components. By creating an accurate scan-derived digital model of the subject, challenging problems can be solved through structure analysis and simulation, such as design of patient-specific implants or surgical plans, optimisation of material designs for target properties, or non-destructive testing of high value parts.

Mostly applications of modern industrial vision system are related to at least one of the following types of inspection: dimensional quality, inspection of surface quality, inspection of correct assembling (structural quality), inspection of accurate or correct operation (operational quality) [ATK17]. In Table 1.1 some of the potential features of an inspected product are reported.

Some examples of industrial vision systems are in food industry to assure the quality of products such as meat, fruit and vegetables, bakery products and more; where machine vision has been used from simple inspections of cans to complex robot guidance, reducing human interaction with the examined goods and assuring faster responses than human beings. Machine vision has an huge impact on electronic industry where it is widely used to inspect Printed Circuit Boards (PCBs) to detect defects, distinguishing and identifying specific PCBs. In automotive industry machine vision is a key technology; it is applied not only on the production line for inspection of car assemblies and sub-components but also in the products itself: 3D-based machine vision methods is also used in automatic driver assistance systems, which include

Dimensional	Dimensions, shape, position, orientation, alignment, roundness, corners	
Structural	**Assembly**	Holes, slots, rivets screws, clamps
	Foreign object	Dust, bur, swarm
Surface	Pits, scratches, cracks, wear, finish, roughness, texture, seams-folds-laps, continuity	
Operational	Incompatibility of operation to standards and specifications	

Table 1.1: Some features of visual inspection.

sensors and cameras installed in vehicles.

1.2 Structure of Image Processing Systems

The function of an image acquisition is to transform the optical image data into an array of numerical data which may be manipulated by the computer. In Figure 1.2 a typical industrial image processing architecture is shown. The structure of an image processing system can be divided into three parts: the sensor, an elaboration system and some communication interface towards other machines or human operator.

This structure resembles a classical architecture for a digital signal analysis, with the only difference that the sensor is composed by one or more cameras and the signal belongs to a two dimensional space. In the case of image processing the signal is represented by a matrix of $N_1 \times N_2$ and the amplitude represents the intensity and therefore is a non-negative value [Bos03]. Generally a computer is employed for processing the acquired images, this is achieved by applying special purpose image processing analysis and classifi-
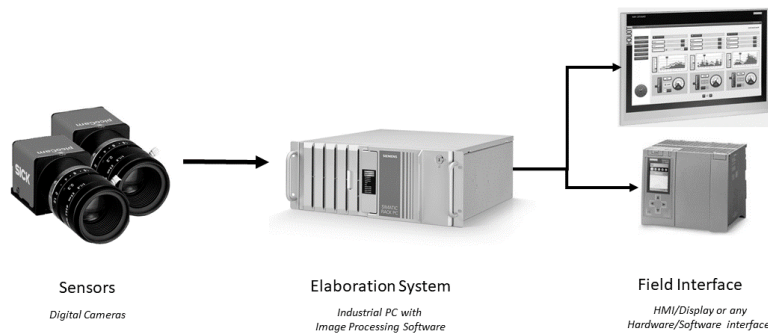
Figure 1.2: Example of an industrial vision system.

cation algorithms. Images are commonly acquired by one or more cameras placed in a fixed position respect to the scene under inspection. The scene is illumiated and arranged in order to facilitate the reception of the image features for processing and classification. Many of the 1-D techniques of digital signal processing can be extended and used for processing images however, many techniques are special for image processing alone.

Classification and interpretation of image are done during the elaboration stage and the results are used to perform the actuation operation. The actuation sub system might interact with the scene in order to adjust or modify any given condition for a better image taking, therefore providing an interaction loop with the original scene.

1.2.1 Sensing Devices

Compared to classical signal acquisition systems, in the case of image processing sensors are analog or digital cameras. Although if cameras are the most common, other image-producing sensors can also be used, e.g. laser and ultrasonic sensors. Scanners of the kind used in graphics design and for the analysis of photographic material, e.g., satellite images, are rarely used in industrial applications, above all because of their slowness. The sensor inside the camera

is a solid-state device which converts the incident light intensity into a digital value that is subsequently processed. The geometrical arrangement of the light sensitive element, also known as pixels, can be in line (line sensors) or more common in a matrix. Unlike an area-scan camera, which acquires a 2D image, a line-scan sensor acquires an image that is only one pixel wide, the image can be then reconstructed an infinite sequence in time of the acquired lines. Image sensors can be classified according to the mode of operation and the technology in CCD (Charge Coupled Device) or in CMOS (Complementary Metal Oxide Semiconductor).

The invention of the CCD sensor dates back to 1969 in Bell Labs and awarded Willard Sterling Boyle and George Elwood Smith the Nobel Prize in Physics in 2009. The CCD sensor consists of two basic parts: the pixel array and the light filter. Pixels are arranged in rows and columns, and each element can be viewed as a tiny solar cell that transforms incident light into electrical charges, allowing its intensity to be measured. The physical principle behind this operation is the photoelectric effect. On each pixel, the filter allows the passage of only certain frequencies of light (usually red, green or blue) and, after a suitable phase of data processing, a color image is obtained. During the integration phase, the conversion of light signal intensity into electric charge takes place. The transformation of the electric charge into an analog voltage signal takes place later in an amplifier, which then sends the signal to the output. The signal is converted into a digital signal by an A/D converter, which is generally located outside the sensor. In order to process the data with a computer, in fact, the initial light signal must be converted into a digital signal. Each sensitive cell contains a photodiode that, exploiting the photoelectric effect, accumulates an electric charge proportional to the incident light. The electrical charge accumulated in all cells is transferred simultaneously to the vertical slide registers. The charges in the vertical registers are then transferred neatly to the horizontal slide register, converted to voltage, and subsequently processed.

(a) Working principle of a CCD pixel.

(b) Working principle of a CMOS pixel.
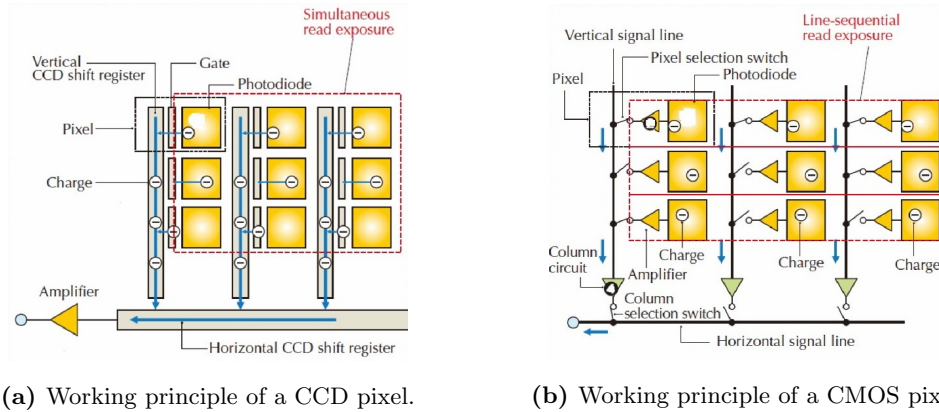
Figure 1.3: Schematic representation of a CCD and a CMOS pixel.

The CMOS Active Pixel Sensor (or Active Pixel Sensor) is an image sensor that, unlike the CCD, contains most of the necessary functionality in each individual pixel and uses CMOS technology. The sensor consists of an integrated circuit and a pixel matrix with the corresponding filter. An analogue-to-digital converter and a digital controller are also housed within the IC. The light arrives through the lens, is processed by the color filter and reaches the pixel matrix. As in the CCD, the accumulation of charge occurs through a photodiode; however, unlike the CCD, the accumulated charge is converted into a voltage by an amplifier located inside the pixel. The digital controller is the set of circuits used to manage and regulate the pixel matrix; among these are the clock generator and the oscillator, which allow the synchronization of work between pixels and impose the integration time.

In Figure 1.3 the working principles of both the CCD ad the CMOS pixel are reported. In the CCD sensor, the digital controller and A/D converter are implemented on an external printed circuit board while CMOS sensors implement all functions on the same chip, allowing for significant space savings. CMOS technology continues to advance in the area of lithography and miniaturization of individual transistors. The structural difference also results in different types of output at each level of the sensor. The pixel of a CCD

sensor provides electrical charges at its output, that of a CMOS sensor provides an analog signal. In CCD sensors, the digital signal is obtained outside the chip; in CMOS sensors, instead, digitization is performed inside the chip. The two sensors also differ in the speed of information transfer within the array. In CCD sensors the information propagates from pixel to pixel and then reaches the output node, which implies longer waiting times. In CMOS sensors, every single pixel has direct access to the output node through the activation of appropriate pass-transistor switches, which results in a higher frame rate. CCD sensors require higher supply voltages than the other type; this inevitably leads to greater power dissipation. Taking advantage of CMOS technology it is possible to achieve a much lower cost, a higher level of integration and lower power consumption. The last two advantages are due to the positioning of the amplifier inside the single pixel. This property, however, also has disadvantages, such as inhomogeneity in the image due to differences in gain between the various amplifiers and the reduction of the area available on the sensor for photo-reception. Moreover, CCD sensors are affected by less noise and their dynamic range is wider than the other type. According to the strengths and weaknesses of each sensor type, the areas of application of one and the other technology are different. Due to their high image quality, CCD sensors are preferred in high-performance cameras and in many scientific and industrial fields such as astronomy, biomedical and spectroscopy. Due to their wide spectrum and high noise rejection, for example, CCD sensors are suitable for astronomical imaging where little light is available. CMOS sensors, on the contrary, are mainly used in the commercial sector, such as in cell phone cameras, which require low power consumption, and in security cameras reserved for video surveillance.

Modern digital cameras not only convert the image into an electrical signal but also are capable of transmitting the image to an elaboration system like a computer. Digital cameras offer high-speed image output; some digital cameras can output data at a rate greater than 100 MB/s. Depending on the

application and on the industry requirements, e.g. the number of images to analyze each second, the size of the image and of course the nature of the elaboration itself, the elaboration system can be a simple industrial computer, embedded systems, or when extremely data-intensive inspection of continuous manufacturing process is required, also parallel computers. By using modern multi-core CPU the majority of the elaboration tasks can be accomplished with standard components; the presence of multiple processing cores enhance the use of multi-threaded algorithms implementations leading to shorter evaluation times [GN12].

Smart Cameras include, in a small size and with a low cost, a computer inside them and represent the preferred choice in modern industrial applications where the elaboration tasks are not computationally demanding, like object detection. These devices can be used without any human interface, like a display, and commonly include several digital input output peripherals to be connected in industrial plant for triggering. In accordance to [ANB10] the first apparition of this term is in the 1975 in [R75] and appeared on the market in the mid 80s; nowadays they have reached a widespread use in industrial applications thanks to their reduced size and high processing capabilities. Smart cameras are especially suited for applications where several cameras must operate independently from any other device, like code reading and verification (barcode, data matrix, QR-Code, OCR), object detection, surveillance systems and other applications.

1.2.2   Image Processing Software

Industrial Vision Systems require a broad spectrum of techniques and disciplines: electronic engineering, mathematics, optics and lighting, mechanical engineering and many others. One of the most important tasks in designing a vision system is of course the development of an algorithm that is capable of extracting from the images the desired information or measure; this is the role of image processing software.

Object

Image
Acquisition

Image
Enhancement

Segmentation

Features
Extraction

Classification

Accept/Reject
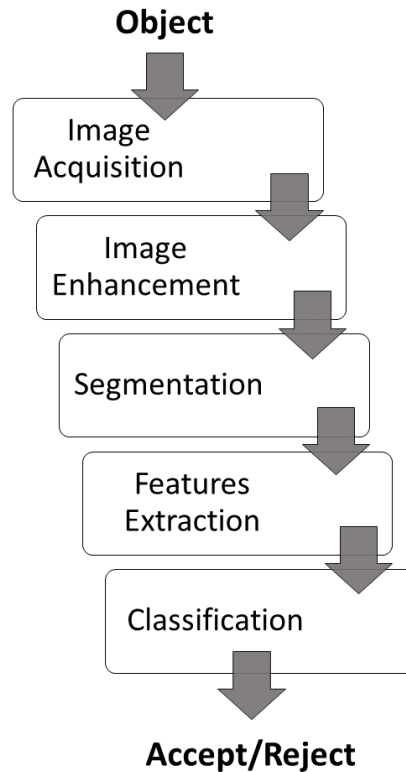
Figure 1.4: Example of an industrial vision software architecture.

The Figure 1.4 reports the view of a general visual inspection software as in [DTP03]. According to the flow represented in the picture the classical process of an image analysis software involves the image acquisition to obtain an image of the object under test; acquisition could be as simple as being given an image that is already in digital form. Generally, the image acquisition stage involves pre-processing, such as scaling [Gon18]. An image enhancement step to improve the quality of the acquired image in order to facilitate the later processing follows the image acquisition, this task is specific to each application. Enhancement techniques are so varied, and use so many different image processing approaches at the point that some enhancing methods can be quite useful in some applications but completely unusable in others. Depending on

the used method they can be divided into spatial domain methods, that directly deals with pixel values, and frequency domain methods, the image is first transferred in to frequency domain by the use of the Fourier Transform and then all the enhancement operations are performed on the Fourier transform of the image and then the Inverse Fourier transform is performed to get the resultant image. Generally the main scope of the image enhancement is to modify the image brightness, contrast or the distribution of the gray levels [MA10]. Some basic operation of image enhancement are:

- creation of the negative of an image; negative images are useful for enhancing white or gray detail embedded in the dark regions of an image. The pixel gray values are inverted to compute the negative of an image.

- Thresholding transformations are particularly useful for segmentation in which we want to isolate an object of interest from a background.

- Logarithmic transformation are particularly useful when the input gray level values may have an extremely large range of values; they map a narrow range of low input gray level values into a wider range of output values, the inverse log transformation performs the opposite.

- Powers-Law transformations, also known as gamma correction, is similar to the logarithmic transformation but makes use of an exponential function that depends on a parameter γ.

- Histogram equalization and histogram matching work on the gray level distribution of the image; the first method tries to stretch out the gray levels in order to produce a more uniformly distributed histogram to obtain a much clearer image, the second realizes an image with a specified histogram, it matches the grayscale distribution in one image with the grayscale distribution in another image.

The image segmentation divides the image into areas of interest and background (region of interest); image segmentation is a crucial procedure for
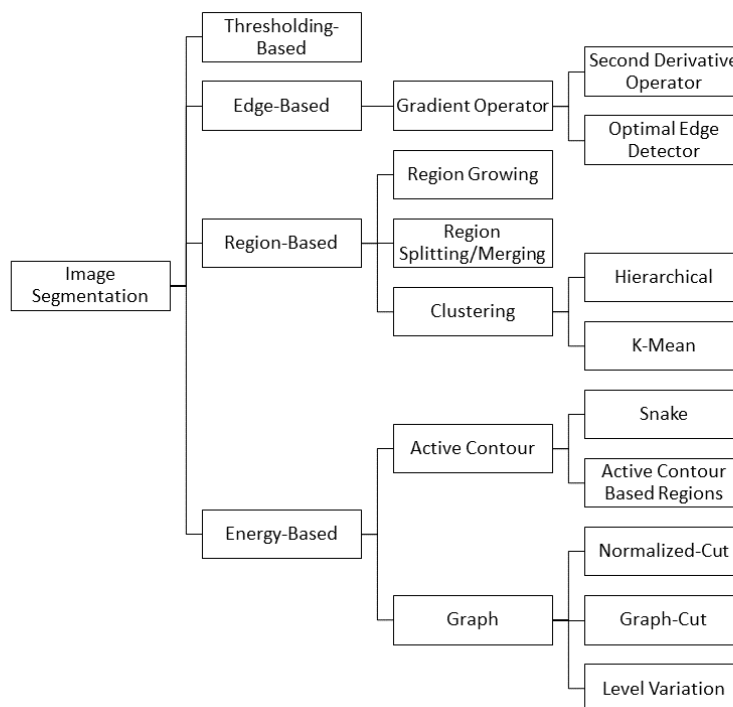
Figure 1.5: Image segmentation techniques categories.

most object detection, image recognition, feature extraction, and classification tasks and many researches have been performed [AS21]. The basic goal of segmentation is to reduce data for an easier analysis process, and it can be applied to a single image or a series of images that form a video. The majority of image segmentation algorithms may be divided into three techniques: boundary-based segmentation, region-based segmentation, and hybrid-based segmentation [ZA15]; moreover segmentation can be accomplished by different categories such as thresholding, edge-based segmentation, region based segmentation and energy based segmentation. In Figure 1.5 a hierarchical classification of image segmentation techniques is reported, a comprehensive review of image segmentation techniques can be found in [MA10].

Feature extraction is the following stage and calculates the values of pa-

rameters that describe each object found during the image segmentation or extracts the measurements from the image. The last step is the classification to determine what is represented by each object and extract a useful result to return to the industrial process.

1.3   Unconventional Measurements based on Image Processing

The previous sections have shown the traditional image processing applications in the industry. As it turns out, image analysis is a direct substitute for applications for which measurements can be made with other tools, such as dimensional measurements made with stereoscopic and non-stereoscopic vision systems. However, there are applications for which, even though there are established instruments capable of directly measuring or determining the desired magnitude, image processing can successfully supplant these.

Among the classic applications, we can certainly include all those of optical inspection on production lines, which directly replace the human's visual capabilities and can perform operations in fractions of a second on moving objects. If we look at computer vision as a field of artificial intelligence [ERDe21] then the spectrum of unconventional applications, both industrial and non-industrial, becomes very broad. The research in imitating the ability of the human being to recognize patterns has become an enabling technology for many applications and the advent of Deep Learning has opened new perspectives pushing the computer vision on more and more diversified applications that go beyond medical and industrial ones but touching also other fields such as archaeology for the restoration of rare writings or the 3D reconstruction of ancient artifacts.

Progress in robots and machine vision has been, and continues to be, driven by more effective ways to process data. Robotic vision is one of the latest innovations in robotics and automation technology; it enables robots and other

machines to see. Visual data processing is a must for robots to perform instructions. Computer Vision used in robotics covers a broader spectrum of disciplines and reappears across categories. From medical science and autonomous navigation, up until nanotechnologies turn to robots to capitalize on daily operations.

Another field where the use of computer vision and image analysis is not entirely conventional is robotics [KD19]. A particular and unconventional example of the use of vision, reported by the authors, is the measurement of steering angles using wheel images, an application already studied in [MJGK12].

The most unconventional image processing use that we are subject to nowadays are face mask detection systems. Due to pandemics, some strict regulations need to be followed to maintain the decorum of the city, state, or country; official authority can not always look for some people not abiding by the rules. Face mask detection has become the solution to this problem. Face mask detection can be done both in images and videos, and different projects have been proposed for the COVID-19 pandemic [HPR$^+$21, KMJC22]. Wearing a face mask is an essential precaution but not the only one and ther applications used image processing to control the Covid-19 spread; an example is the measure of social distancing to slow down the spread of the virus [SMNS21]. In this context, the use of cameras demonstrated to be a better solution to the use of sensors that re handed out might act as a medium for the virus to spread [ZD21, GEAG20].

"Unconventional measurements" include all those measures for which there are conventional and classical solutions using well-known measurement tools. However, the exact measurement can be obtained by the use of image processing has a contribution if not better in terms of accuracy and or sensitivity makes the measurement feasible by offering alternative performance or allowing to analyze the problem in a different form than the more conventional methods.

References

[AE15]   Basavaraj Anami and Mahantesh Elemmi. A rule based approach for classification of shades of basic colors of fabric images. *International Journal of Signal Processing, Image Processing and Pattern Recognition*, 8:389–400, 02 2015.

[Ale83]   I. Aleksander. *Artificial Vision for Robots*. 01 1983.

[ANB10]   Ahmed Nabil Belbachir Ahmed Nabil Belbachir, Peter Michael Gobel. *Smart Cameras*. Springer US, 1 edition, 2010.

[AS21]   Salwa Abdulateef and Mohanad Salman. A comprehensive review of image segmentation techniques. *Iraqi Journal for Electrical and Electronic Engineering*, 17:166–175, 12 2021.

[ATK17]   Aparna, Dr.Ritula Thakur, and Pradeep Kumar. An overview of industrial vision systems. *International Journal of Advance Research and Innovative Ideas in Education*, 3:201–207, 2017.

[BDG94]   Bruce Batchelor, Michael Daley, and Eric Griffiths. Hardware and software for prototyping industrial vision systems. 10 1994.

[BGB97]   Dr Paul F. Whelan Bruce G. Batchelor. *Intelligent Vision Systems for Industry*. Springer-Verlag London, 1 edition, 1997.

[Bos03]   Tamal Bose. *Digital Signal and Image Processing*. Wiley, 1st edition, 2003.

[BW94]   Bruce Batchelor and Paul Whelan. *Selected papers on industrial machine vision systems*. 01 1994.

[CD13]   Carsten Garnica Christian Demant, Bernd Streicher-Abel. *Industrial Image Processing: Visual Quality Control in Manufacturing*. Springer-Verlag Berlin Heidelberg, 2 edition, 2013.

[CH82] Roland T Chin and Charles Harlow. Automated visual inspection: A survey. *Pattern Analysis and Machine Intelligence, IEEE Transactions on*, PAMI-4:557 – 573, 12 1982.

[CS18] Christian Wiedemann Carsten Steger, Markus Ulrich. *Machine Vision Algorithms and Applications, 2nd Edition*. Wiley-VCH, 2 edition, 2018.

[DTP03] R J Alcock Duc T. Pham. *Smart Inspection Systems: Techniques and Applications of Intelligent Vision*. 2003.

[ERDe21] Matthew Turk (editor) E. R. Davies (editor). *Advanced Methods and Deep Learning in Computer Vision (Computer Vision and Pattern Recognition)*. Academic Press, 1 edition, 2021.

[GEAG20] Abdalla Gad, Gasm ElBary, Mohammad Alkhedher, and Mohammed Ghazal. Vision-based approach for automated social distance violators detection. In *2020 International Conference on Innovation and Intelligence for Informatics, Computing and Technologies (3ICT)*, pages 1–5, 2020.

[GN12] Chetan Gowda and Prabhakar Neelawani. parallel architecture for image processing. 07 2012.

[Gon18] Richard E. Gonzalez, Rafael C.; Woods. *Digital image processing*. Pearson, 4th ed. edition, 2018.

[HPR⁺21] G K Jakir Hussain, R Priya, S Rajarajeswari, P Prasanth, and N Niyazuddeen. The face mask detection technology for image analysis in the covid-19 surveillance system. *Journal of Physics: Conference Series*, 1916(1):012084, may 2021.

[JL17] Bruce Hasegawa Jack Lancaster. *Fundamental Mathematics and Physics of Medical Imaging*. Series in Medical Physics and

Biomedical Engineering. CRC Press, Taylor and Francis Group, 1 edition, 2017.

[KD19]   Paulo Roberto Gardel Kurka and Aldo André Díaz Salazar. Applications of image processing in robotics and instrumentation. *Mechanical Systems and Signal Processing*, 124:142–169, 2019.

[KJFA20] Yassin Kortli, Maher Jridi, Falou, and Mohamed Atri. Face recognition systems: A survey. *Sensors*, 20:342, 01 2020.

[KMJC22] Sohit Kummar, Asutosh Mohanty, Jyotsna, and Sudeshna Chakraborty.   Real time face mask detection using google cloud ML and flutter. *Journal of Physics: Conference Series*, 2161(1):012020, jan 2022.

[MA10]   Raman Maini and Himanshu Aggarwal. A comprehensive review of image enhancement techniques. *CoRR*, abs/1003.4053, 2010.

[Mes21]   Luca Mesin. Biomedical image processing and classification. *Electronics*, 10:66, 01 2021.

[MJGK12] Carlos Roberto Mingoto Junior and Paulo Roberto Gardel Kurka. Guidelines to specify a camera for computer vision measurement of vehicle suspension alignment angles based on the desired sensibility. In *2012 Symposium on Photonics and Optoelectronics*, pages 1–3, 2012.

[PG21]   Ewa Pietka and Arkadiusz Gertych. Advances in biomedical image processing. *Computerized Medical Imaging and Graphics*, 89:101891, 03 2021.

[R75]   SCHNEIDERMAN R. Smart cameras clicking with electronic functions. *ELECTRONICS; U.S.A.; DA. 1975; VOL. 48; NO 17; PP. 74-81*, 1975.

[SMNS21] G V Shalini, M Kavitha Margret, M J Sufiya Niraimathi, and S Subashree. Social distancing analyzer using computer vision and deep learning. *Journal of Physics: Conference Series*, 1916(1):012039, may 2021.

[Sue09] Paul Suetens. *Fundamentals of Medical Imaging*. Cambridge University Press, 2 edition, 2009.

[TA05] Ajoy K. Ray Tinku Acharya. *Image Processing: Principles and Applications*. Wiley-Interscience, 2005.

[TVTV99] Prinya Tantaswadi, J. Vilainatre, N. Tamaree, and P. Viraivan. Machine vision for automated visual inspection of cotton quality in textile industries using color isodiscrimination contour. *Computers and Industrial Engineering - COMPUT IND ENG*, 37:347–350, 10 1999.

[WGW$^+$95] Bruce Wilkie, B. GRIFFITHS, Y. WANG, P. NORGATE, and P. SILVERWOOD. An ai vision system for the inspection of complex coloured objects. *International Journal of Production Research - INT J PROD RES*, 33:2633–2647, 09 1995.

[YT19] Juri Yanase and Evangelos Triantaphyllou. A systematic survey of computer-aided diagnosis in medicine: Past and present developments. *Expert Systems with Applications*, 138:112821, 07 2019.

[ZA15] Nida Zaitoun and Musbah Aqel. Survey on image segmentation techniques. *Procedia Computer Science*, 65:797–806, 12 2015.

[ZD21] He Ziran and Naim Dahnoun. A contactless solution for monitoring social distancing: A stereo vision enabled real-time human distance measuring system. In *2021 10th Mediterranean Conference on Embedded Computing (MECO)*, pages 1–6, 2021.

[ZL14] Hang Zhang and Daoliang Li. Applications of computer vision techniques to cotton foreign matter inspection: A review. *Computers and Electronics in Agriculture*, 109:59–70, 11 2014.

Chapter 2

Case Study: Drill Bit Wear Monitoring

Monitoring tools and inserts is a critical task in the manufacturing industry of any kind; this is one of the key points for production quality control and the reduction of the total cost of the manufactured goods. Worn tools can cause damage not only to goods but also to the machining, causing unscheduled stops due to equipment breakage or deterioration. In this chapter, an example of visual inspection for industrial tooling will be reported.; in particular, the drill bit wear will be considered. Drill bits are used in any manufacturing industry, starting from woodworking to heavy-duty iron working and also the electronic industry for PCBs production.

2.1 Industrial Tool Wear Monitoring

In aerospace applications, the use of reinforced carbon fibre composite laminates is increasingly common due to their superior mechanical properties, associated with their low weight, if compared to other types of materials. These laminates are difficult to process due to the material's intrinsic anisotropy and inhomogeneity. Machining operations on these materials, with particular reference to perforation, are critical and can cause damages when the laminate is

subject to heavy stress. The stresses and vibrations during the drilling process can cause widespread damage that compromises the mechanical properties of the finished piece. However, composite materials' drilling is a conventional machining process in the aerospace industry. Composite material parts are assembled to other parts by mechanical joints due to the difficulties in making welds or adhesive joints. The holes reduce the resistance of the laminate to stress and are subjected to stringent quality requirements.

The holes must be in the correct position regarding the geometric requirements, have the right shape, and the diameter's expected tolerance. Other quality parameters are related to surface integrity and roughness. When drilling, both the shear strength and friction between the drill bit and the composite piece can cause various types of damage such as delamination, blurring, and chipping. Delamination caused by perforation is one of the most commonly used parameters for evaluating hole quality as it affects the structural integrity of the laminate and can deteriorate long-term performance.

The drill bits' wear measurement represents a critical point in industrial production processes and reflects the tools' average lifetime. An excessively worn drill bit can damage the perforated material's surface and the size of the drilled hole. It is necessary to develop quantitative tool wear measurement techniques to determine the precise timing for tool replacement. In this respect, several studies suggest techniques based on image processing [RJO05, JKK05, KML+02].

2.1.1   State of The Art

A digital image analysis method is presented in [CAT17]. It measures the relevant parameters representing the quality of the drilled hole, focusing attention on the hole geometry and the measurement of selected indices that characterize the relative delamination phenomena both at the entrance and at the hole exit. The results show that the diameter generally decreases as the number of holes increases. The delamination at the hole exit is more correlated to tool

wear progression during drilling.

Computers and sensors control the wear monitoring of components and mechanical tools. Tool wear is caused by physical and chemical interactions between the drilling object and the work piece. It can be described as the removal of small pieces of material from the cutting edge of the tool as a result of these interactions. The component wear' measuring methods can be divided into direct and indirect methods [KB97]. Indirect methods measure the degree of tool wear through sensors while generate signals that indirectly provide information on the state of the object, such as force sensors, vibrations, or acoustic emissions. Indirect measurement techniques generally require the reception of continuously acquired signals. They are widely used thanks to their ease of installation on industrial machines, which does not affect the machinery's function and does not alter the production process. Indirect measurement methods can use several sensor and principles to detect the wear of the tool:

- Torque measurement and push force measurement require special tooling of the drill system and can influence the dynamics and the overall performance and characteristics of the machining.

- The acoustic emission (AE), also known as "stress wave emission" or "microseismic activity", is a phenomenon of sound and ultrasound wave radiation where elastic energy is released in the form of mechanical vibration from a material (tool, workpiece, machine body) as it undergoes deformation and fracture processes [YON95]. Acoustic emission sensors are generally more expensive and require a higher sampling rate and computing performance resolution than industrial accelerometers [MKJ00].

- Accelerometers are easy to mount and use on industrial machinery. They do not compromise the drilling system's rigidity, and they present good immunity to electromagnetic interferences. They are cheap and can be

easily substituted.

To overcome the single sensor's weakness a multi-sensor platform can be used as described in [DPB$^+$16], in indirect measurement. A comparison between sensors sensitivity and machining precision is reported in Figure 2.1.
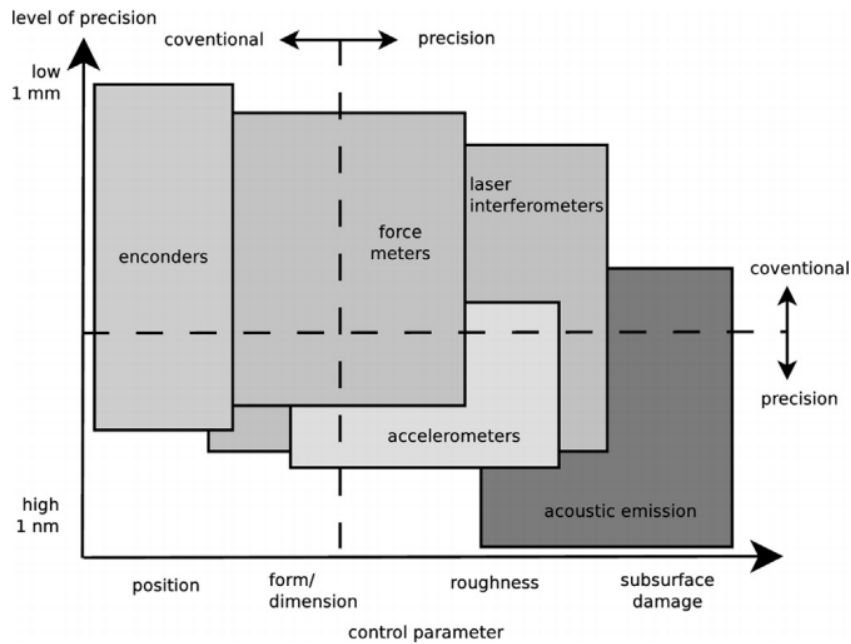
Figure 2.1: Sensor sensitivity to different levels of machining precision and error control parameters. Image taken from [DPB$^+$16].

The amount of data produced by indirect methods is so large that it requires neural networks and high-performance computing devices to be analyzed. Regarding this point, a comparison between different architectures of a multilayer feed-forward neural network is presented in [AM03]. They use a training and posterior propagation algorithm for monitoring the wear conditions of a twist drill. The algorithm uses the vibration trace as the only source of information on the machining process. At the input to the neural network, different tip wear conditions are introduced, some of which are represented in Figure 2.2. The frequency-domain characteristics, such as average harmonic

wavelet coefficients and the peaks of the spectrum at maximum entropy, are
more efficient in training the neural network than statistical moments in the
time domain. The results suggest that vibrational signals have a significant
impact on tool condition monitoring and manufacturing process diagnostics.

(a) Chisel wear.   **(b)** Flank wear.   **(c)** Edge fracture.

(d) Crater wear.   **(e)** Outer corner wear.
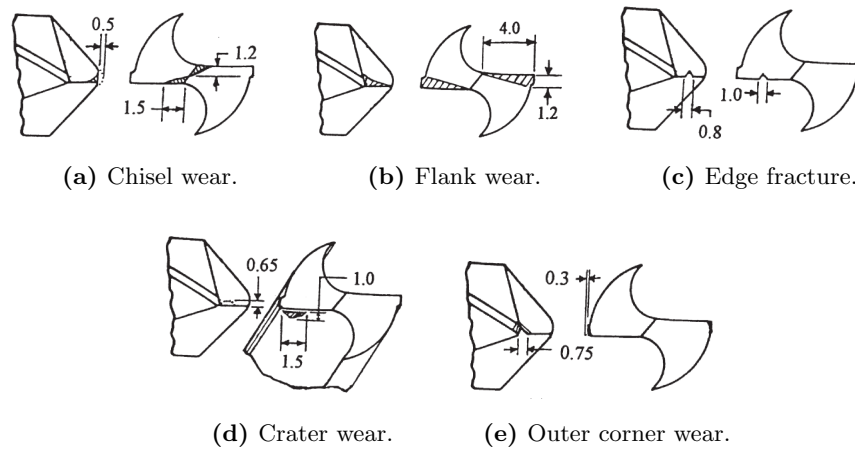
Figure 2.2: Artificially induced drill wear. Drawings taken from [AM03].

On the other hand, the direct method allows information to be obtained
directly by analyzing the images of the drill bit. This method provides im-
mediate evaluation of the actual wear of the objects that may require their
removal. The measurement methods most used in the inspection processes of
mechanical components are the direct ones. With direct measurement, the tool
blade is monitored using, for example, an artificial vision system, an optical
microscope, or a touch sensor.

Advances in computer vision and image processing technology have led to
the development of various vision sensors that can be used to obtain infor-
mation about the drilling tool and the perforated surface. One of the most
important advantages of machine vision-based measurement systems is that
the drill bit is not in permanent contact with the machined part. Monitoring
can be achieved with vision systems without any physical contact.

An automatic optical inspection system for drilling tips for PCB (Printed

Circuits Boards) is presented in [ZLYS06]. A specifically designed lighting system (Figure 2.3b) ensures high image quality of the tips. A modified version of the SUSAN (Small Univalue Segment Assimilating Nucleus) algorithm is used. Through the use of a differential operator based on the spatial moment, it is possible to obtain a precision on the position with an uncertainty lower than a pixel. The algorithm returns curves that discreetly approximate the edges of the cutting surfaces of the tip. The angles of the tip are instead determined with suitable precision from the intersections of the extrapolated curves. Once all inspection items have been identified, flaw detection is performed on the tip blade surface. The results show that adopting the automated optical tip inspection method for PCBs results in increased product quality and reliability. The small size of the printed circuits and their respective tips, however, make it necessary to use acquisition devices with a very high resolution.
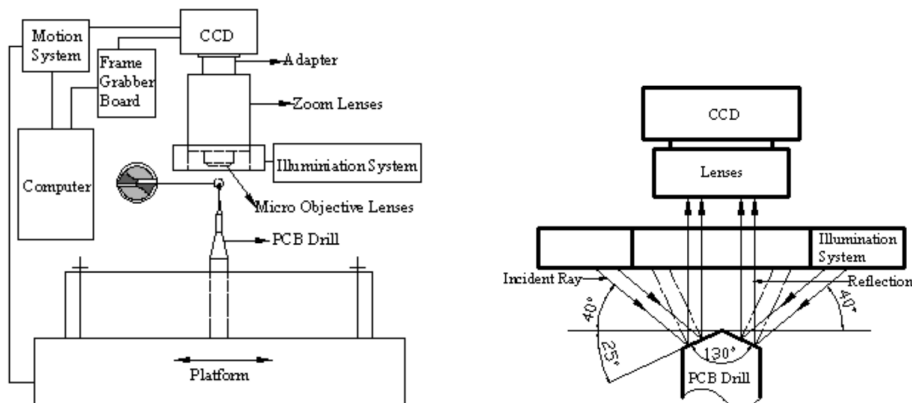
(a) Block diagram of the Automatic Optical Inspection (AOI) system for PCB drill bit proposed in [ZLYS06].

(b) Proposed illumination system.

Figure 2.3: Automatic Optical Inspection proposed by *Zhang et al.* Pictures taken from [ZLYS06].

In most vision-based measurement techniques, the drill bit is framed from the front. The authors of [HSH19] present an inspection system in which
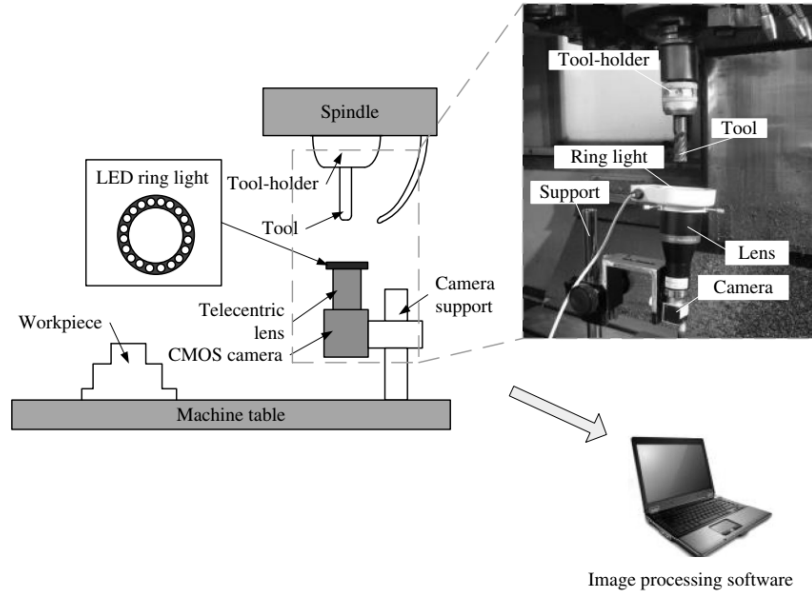
Figure 2.4: Block diagram of the online tool wear inspection system proposed by *Hou et al.* in [HSH19].

the image acquisition module is equipped with a 14 Mpixel C-MOS camera, a bi-telecentric lens, and a LED ring illuminator with adjustable intensity, Figure 2.4. The image processing system includes a comparison algorithm and the corresponding graphic interface with the user. The segmentation of the image is carried out through an adaptive classification of the connected domain. The edges of each blade are rotated on the basis of the main components analysis. The thicknesses of each cutting edge are calculated and the maximum value of these widths is used as an indicator of tool wear through the approximation to the least-squares. In the case of complete wear or breakage of the component, the absolute value of the error on the measurement is less than $0.057\,\mathrm{mm}$ and is due to the irregularly reflected light. The system guarantees high speed and precision in the inspection of the cutting tool used in aerospace production. The use of a very high resolution camera and telecentric optics, however, can require high and, sometimes, excessive costs.

It is possible to analyze the drill bit from the front side and from the lateral side, and several researches have been published. *A. Volkan Atli and M. Sonmez* in [AUES06] propose a system for monitoring the conditions of drilling tools based on artificial vision conducted with a high-speed CCD camera, placed on the side of the tip. Canny's algorithm [Can86] is used to extract the necessary information from the acquired images, particularly suitable for detecting contours. This technique is quite sophisticated but provides a good compromise between noise reduction and image edge localization. However, to obtain a measure of the tip wear, a linearity deviation metric (DEFROL) is proposed, which measures how far the contour of the tool flank differs from the straight line. The authors carried out the tests on 40 tips with various diameters (6, 8, 9 and 12 mm) and all objects were classified correctly. The average value of the measurement carried out with the DEFROL technique varies linearly as the tip diameter increases and this method also allows for quick and effective visual diagnostics. It is not certain, however, that the outline of the image always follows a linear trend because the tips used in the drilling processes can take on different shapes. The lateral profile also varies with every slight rotation the object undergoes around its axis of symmetry. The inspection of the tip and the estimation of wear focus mainly on the cutting plane, which is determined if the camera that acquires the image to be processed is placed in front of the tip. As for the optical control of the tips in the production of printed circuits, the increasing integration density entails the microminiaturization of the drilling tips and the need to resort to a vision system with an increasingly high resolution. When the diameters of the tips reach the decidimes or even the hundredths of a millimeter, we resort to the use of microscopes for image acquisition. If the cutting plane cannot be segmented exactly, it is impossible to obtain an accurate measurement result with the proposed method.

Most image edge detection algorithms work well if the cutting plane is clear and the tip is clean. During the manufacturing processes, however, traces of
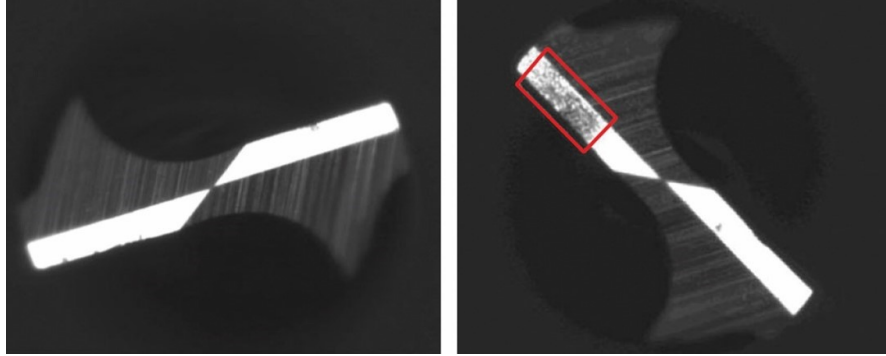
Figure 2.5: Drill bit comparison: clean on the right.

dust and smudging stains may be deposited on the tips, which camouflage the cutting plane and cause errors in the analysis of the single image. As shown in Figure 2.5, it is possible that in the acquired image, the intensity level of the pixels corresponding to the stained part is closer to the level of the pixels in the background rather than to that of the cutting surfaces on which the measurement should be conducted, in these cases conventional segmentation methods don't work.

The authors in [DCS10] propose an iterative algorithm that uses a series of levels to segment the cutting plane and determine the blades' surfaces without the dirty regions affecting the measurement. This algorithm is based on the idea to start from a zero-level function, defined in a space of a higher dimension than that of representing the image contours, and to follow the evolution of the function through a discrete differential equation. It is a flexible method that can include additional features, and that returns good results as the number of iterations increases; however, this strategy may require too much processing time and excessive computational complexity.

For a feature of the object under inspection to appear in the image acquired by an optical measurement system, the object must be suitably illuminated. In industrial vision systems, light must be supplied in a controlled manner so as to highlight the characteristics of interest and reduce the presence of unwanted

ones. Lighting is one of the most critical aspects of an automatic vision system, for this reason the choice of the lighting method is extremely important. *R. Ramzi and E.A. Bakar* [RB18] propose an optical inspection method for the wear of the drill bits used in the assembly sector of the aeronautical industry, from which important considerations can be drawn on the orientation of the rays illuminating the surface of the focus, on the nature of the light and on the alignment of the tool with respect to the objective. The monitoring system described by them consists of a very complex hardware part, composed of a digital microscope for image acquisition with its own lighting, two strips of LED illuminators to further improve the image quality, pair of servomotors used to adjust the rotation angle of the supplementary illuminators and by a spindle that fixes the position of the drill bit in order to align it with the microscope. The system used is shown in Figure 2.6. The tip is placed in a vertical position and framed from top to bottom. In this way, the drill bit axis of symmetry coincides with the image acquisition instrument's optical axis, whether this is a microscope or a generic camera. The drill bit image can be divided into different regions: the cutting blade and the chisel edge are the two main cutting edges of the four edges into which the cutting plane is divided. The cutting blades correspond to the edges through which the tip removes material from the perforated surface. The edges of the chisel are placed on the line of intersection between the cutting surface and the lateral surface.

2.2   Image Based Drill Bit Wear Estimation System

To solve the problem of drill bit inspection the proposed solution uses a custom designed lighting and image acquisition system. They were set up on an optical bench, so as to ensure the alignment of the tip with the camera and the symmetry of the supports with respect to the optical axis. The supports that make up the system have been physically sized and made through a 3D
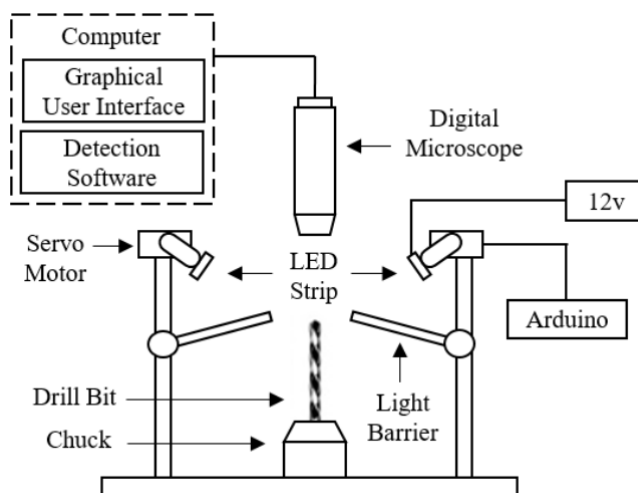
Figure 2.6: Schematic representation of the system proposed in [RB18].

printer, using PLA (polylactic acid), as in Figure 2.7.

It was experimentally found that the light produced by a single white LED is able to uniformly illuminate the region of a cutting blade when the orientation of this region falls within a certain angular range and does not excessively stand out the remaining regions of the surface of the drill bit. A specific ring illuminator was designed, whose operating principle adopts the image computation technique. The illuminator consists of a support in the shape of a circular crown, specially printed and perforated in 16 points; inside each of these a white light LED was inserted. The emission of the single LED, due to the lens in the shape of a spherical cap, is of the radial type but each hole is inclined in such a way that the direction of its axis intersects the optical axis at the point where the drill bit is in focus. The illuminator is capable of producing different light patterns, depending on the state of the LEDs at each step of the acquisition; some patterns are reported in Figure 2.9.

Taking advantage of the computational image processing technique, the LEDs making up the system are turned on sequentially, and at each step of the sequence, an image is acquired. The 16 images obtained following this
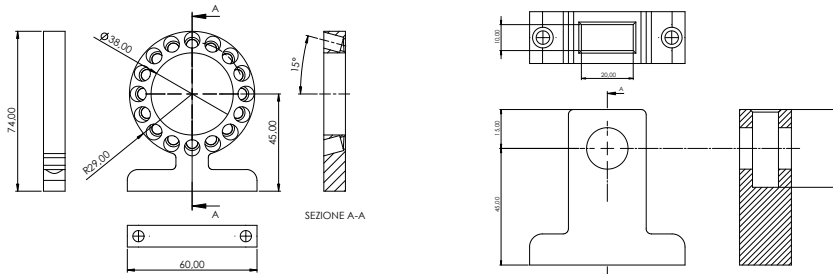
(a) Drawing of the illumination system. All the measures are in mm.

(b) Drawing of the drill bit support piece. All the measures are in mm.
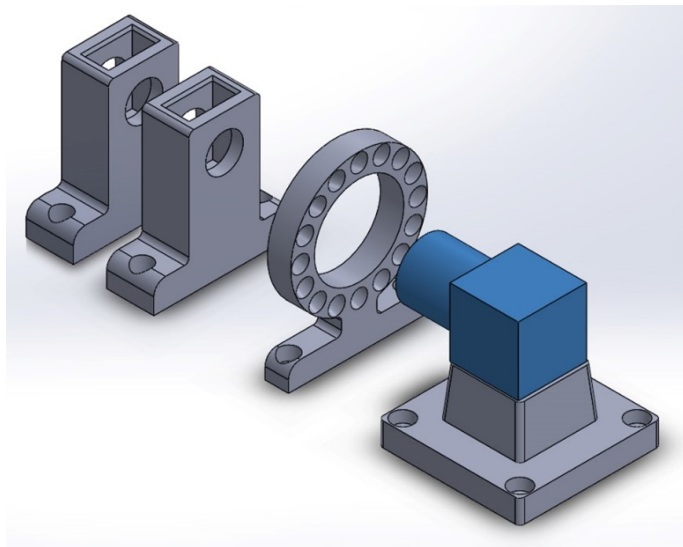
(c) 3D CAD representation of the assembly of the measurement system.

Figure 2.7: Drawings and 3D model of the proposed acquisition system.
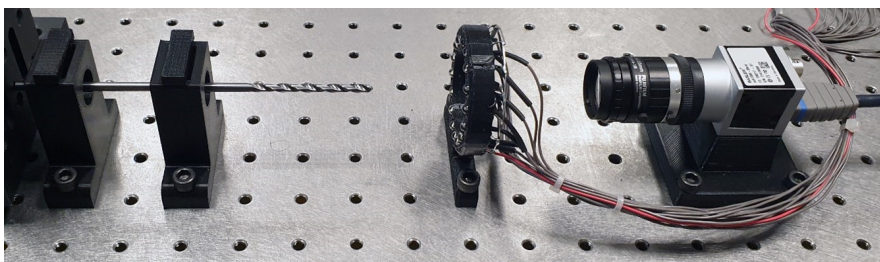
Figure 2.8: Realized measurement system mounted on an optical bench.
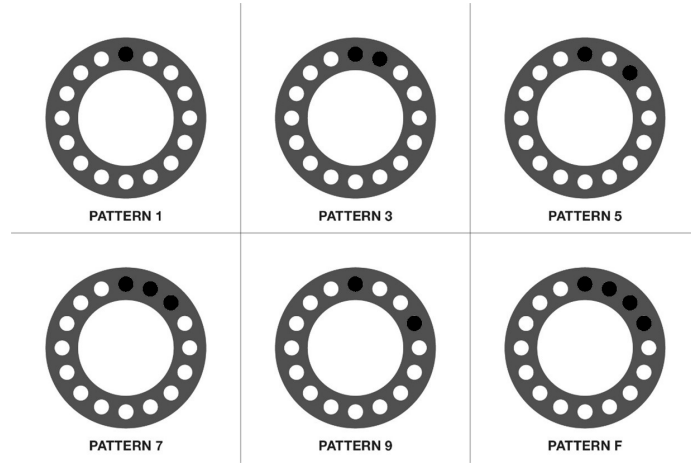
Figure 2.9: Examples of different light patterns on the illumination system.

procedure represent the front surface of the tip subjected to the measurement, always oriented in the same position but always illuminated from a different direction. The images are all different from each other. By choosing a generic pair from the overall set of 16 elements, the two images can differ even only for a limited number of pixels. Some images highlight the details sought or one of the two cutting surfaces; the others contain superfluous information for the purpose of the measurement. The designed lighting system allows to vary the source's angle with a resolution equal to one sixteenth of the round angle, that is, about 23°. This rotation step guarantees at least the presence of a pair of images in which the first and second cutting blades stand out respectively. By appropriately processing the 16 images, it is possible to obtain a definitive image, whose amount of information is much greater than a single acquisition of the sequence.

In Figure 2.10 three examples of the computational image with different illumination patterns are reported: in the first example (Figure 2.10a) the pattern with a single led is used; the light in the image is not sufficient and some regions of the drill bits are in shadow. In the second image (Figure 2.10b) and third image (Figure 2.10c) two and three leds are lighted simultaneously
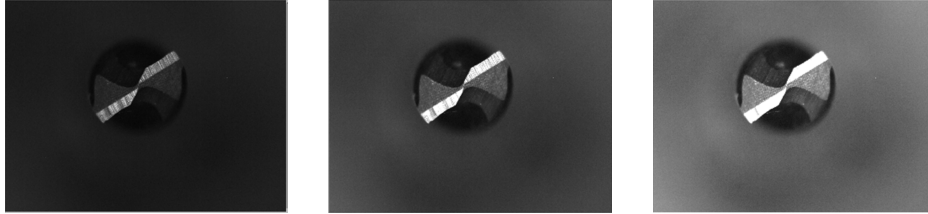
(a) Illuminator pattern n. 1. (b) Illuminator pattern n. 3. (c) Illuminator pattern n. 7.

Figure 2.10: Examples of different light patterns.

respectively; the best result is obtained with the pattern n. 3. Other experiments were done to show the best LEDs configuration; in Figure 2.11 a comparison of illuminator light pattern n. 7 and illuminator light pattern n. 9 are reported. The Figures 2.11c and 2.11d report the histogram of the single image captured while the Figures 2.11a and 2.11b the relative computational images.
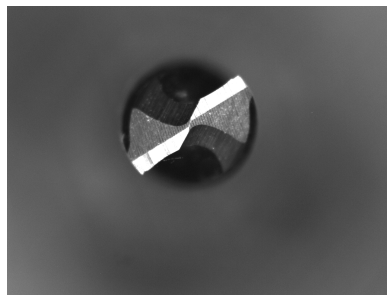
(a) Computational image obtained with pattern n. 7.
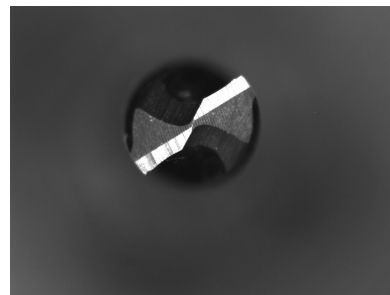
(b) Computational image obtained with pattern n. 9.
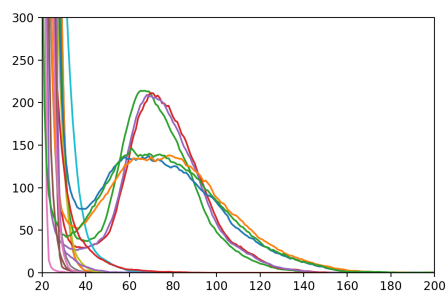
(c) Histogram for pattern n. 7.
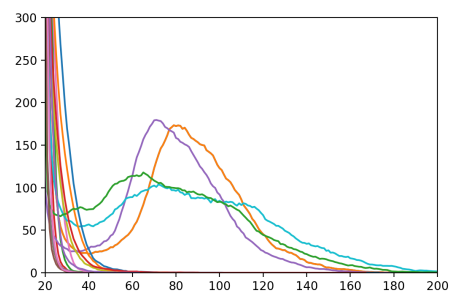
(d) Histogram for pattern n. 9.

Figure 2.11: Examples of computational image and histogram of the single images for light patterns n. 7 and n. 9.
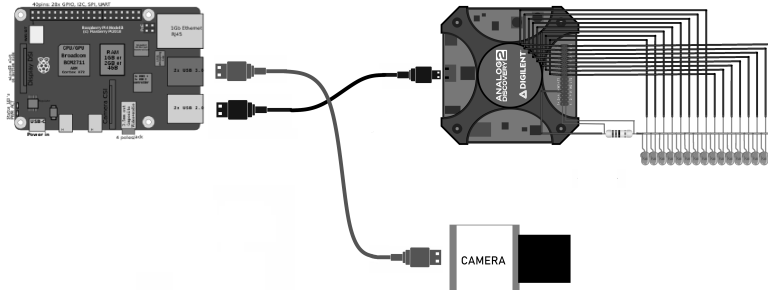
Figure 2.12: Block Diagram of the measurement system.

In the first prototype the measurement system was composed by the custom illuminator driven by an Analog Discovery Board and a Raspberry PI, a low-power single board PC that controls the system. In Figure 2.12 a block diagram of the system is reported while in Figure 2.8 a picture of the experimental setup on an optic-bench.

The goal of the implemented algorithm is to extract the two geometric shapes of the surfaces of the cutting edges, aligned on the transverse axis and arranged symmetrically with respect to the tip centre.

During its operation, the drill bit rotates clockwise around its axis of symmetry. Therefore, in the image depicting the tip, the rotation takes place counter-clockwise and the wear of the cutting edge is reflected directly on the cutting blade. The blade profile is expected to vary depending on the wear of the tip and the thickness of the surface.

The algorithm, reported in the form of a block diagram in Figure 2.13 can be divided into several steps: computation, thresholding, RoI extraction, drill bit axis extraction and profile extraction. In the following the steps will be analysed.

1. The computation of the sixteen images is based simply on the arithmetic sum; an example of the original images is reported in Figure 2.14a, they were acquired using the light pattern n. 3 with reference to Figure 2.9.
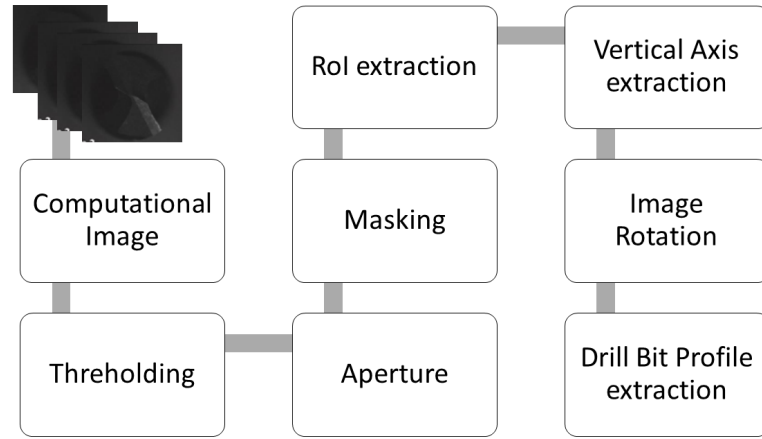
Figure 2.13: Block diagram of the blade profile extraction algorithm.

The camera used is monochromatic, so each image is in greyscale and the value of the single pixel varies from 0 to 255. The value 0 corresponds to black while the value 255 corresponds to white. All the images have the same size, the pixels are arranged in a two-dimensional matrix with 960 rows and 1280 columns. The arithmetic sum of sixteen greyscale images yields an overall image in which the (i, j) element has a value given by the sum arithmetic of the sixteen values of the pixels corresponding to the same position. Since the maximum limit of the grey level is equal to 255, when the sum of the sixteen values exceeds this number it is approximated precisely to 255. If the brightness of the lighting system did not guarantee a good contrast of the single image, the arithmetic sum would return as a result an incorrect image.

$$I_C(i, j) = \Gamma \sum_{k=1}^{16} \alpha_k I_k(i, j) \tag{2.1}$$

The equation 2.1 expresses the calculation of the computational image where $I_k(i, j)$ with $k = 1..16$ are the original images, α_k is a weight given to each image and Γ is a threshold function applied to each pixel of the

image in order to limit the value to 255:

$$\Gamma(x) = \begin{cases} x & \text{if} \quad x < 255 \\ 255 & \text{if} \quad x \geq 255 \end{cases} \qquad (2.2)$$

In Figure 2.14a the single images use to compute the image Figure 2.14b are reported.

2. A threshold operation is performed to obtain a binary image. The choice of the threshold value depends on the computed image's pixel values and can be conducted by analyzing the histogram of the computed image. The over sizing of the field of view, necessary to make the system adaptable to larger sized tips, means that the tip image occupies a limited region of the overall size. The excessive number of pixels belonging to the background makes the histogram single-mode.

3. The angular position of the drill bit is arbitrary and not controllable. A scan is carried out on the binary image without isolated points to determine the pixels' coordinates corresponding to the extremes of the drilling tip in each of the four directions. A rectangular mask is then applied, the sides of which correspond to the two pairs of abscissas and ordinates found by scanning. Subsequent processing is carried out exclusively on the pixels inside the mask to reduce the algorithm's computational complexity.

4. A straight edge search is performed on the grey scale image since it contains information on the gradient. The transverse axis's position on which the two cutting surfaces lie and with respect to which the blades are aligned is sought. The value to be calculated is the orientation angle of the axis with respect to the Cartesian plane on which the image of the drill bit lies.

5. Each image is rotated clockwise by an angle equal to the value returned in the previous step. In this way, the two cutting edges are aligned

vertically, and, in the rotated images, the rectilinear contour coincides with a central column. To trace the two cutting edges' profiles with respect to its transverse axis, simply adds the pixels arranged on the lines, as

$$h(j) = \sum_i I_F(i,j) \tag{2.3}$$

where $h(j)$ is a single point of the reconstructed profile and represents the height of the profile, and I_F is the computational image filtered with the previous steps.

In Figure 2.15 different images of a drill bit analysed using the previous procedure are reported.
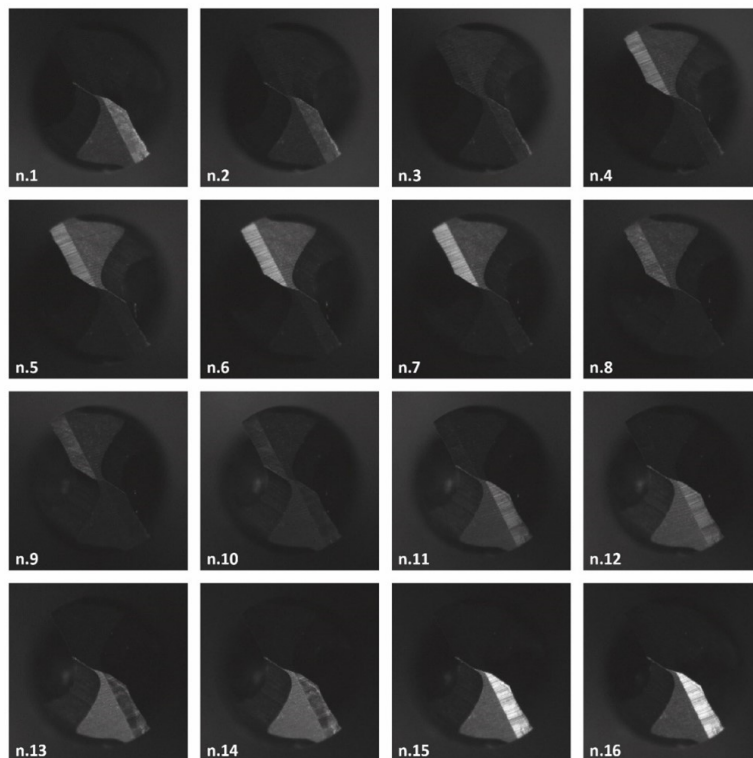
(a) Example of acquired images with a specific light pattern.
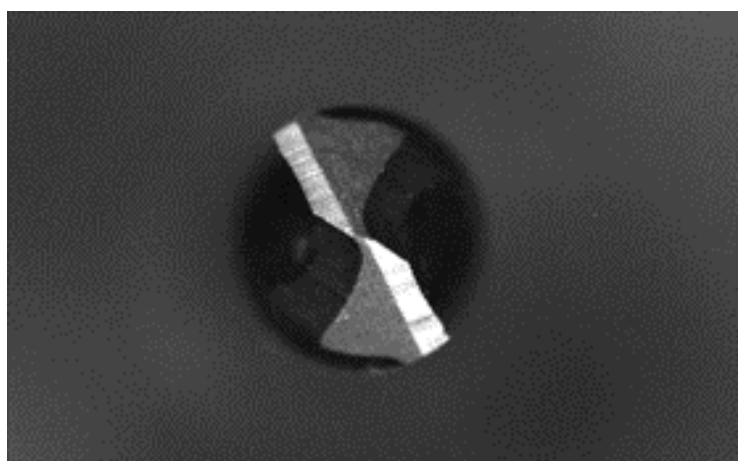
(b) Example of computed drill bit image, trimmed for graphical reasons.

Figure 2.14: Example of acquired images in 2.14a and obtained computational image 2.14b.

(a) Original computational image.

(b) Masked image.

(c) .

(d) Erosion.

(e) Cropped image.
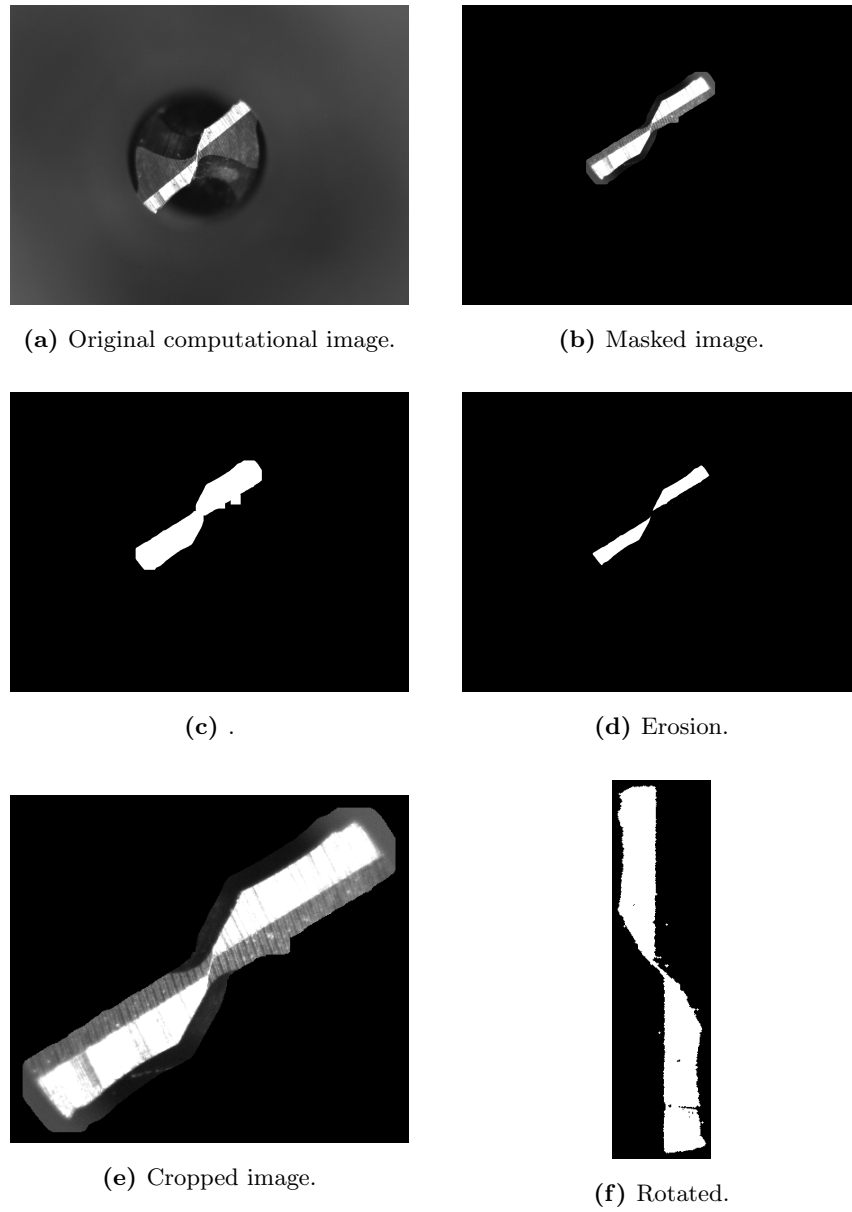
(f) Rotated.

Figure 2.15: Example images of the steps to obtain the rotated image.

Another approach to calculate the rotation of the drill bit is the use of the
Radon transform [vGLHVV04, LHvGVVV04]. Radon transformation projects
the image on a line with a predetermined direction and the result is a curve
that describes the light intensity on that direction Figure 2.16; this opera-
tion can be done with angles from $0\,\mathrm{deg}$ to $180\,\mathrm{deg}$ with a fixed increment.
For each transform the maximum value is calculated and then the maximum
angle is obtained as the angle of the rotation that establishes the maximum
illumination value.
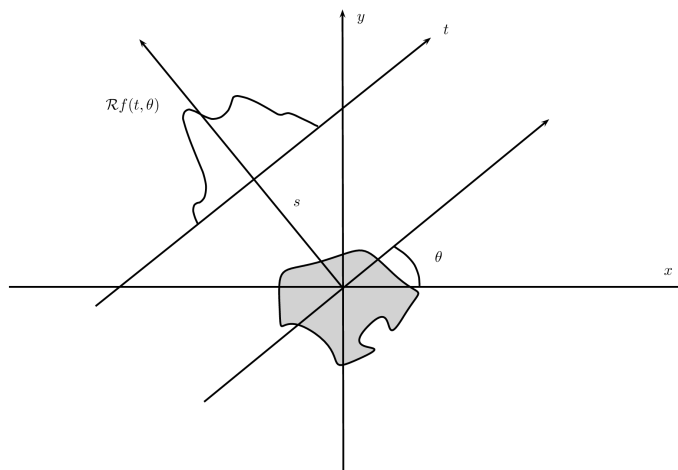
Figure 2.16: Principle of the Radon transform.

The Hough transform provides a technique for recognizing particular con-
figurations of points in the image, such as segments, curves, or other fixed
shapes. The basic principle is that the shape sought can be expressed by
a known function using a set of parameters. As an example if the straight
line is considered, with equation $y = ax + b$, it is entirely defined by its two
parameters (a, b); if, instead, we consider the line equation in a polar plane
$(\rho = x cos\theta + y sin\theta)$ then the parameters become (ρ, θ). Given the shape of
interest and its representation it is possible to find a transformation of the
image plane to the parameter space. In this way, a particular instance of a
line is represented by a point in the parameter space. In the image plane,

a point is identified by the intersection of multiple lines; thus to each point P corresponds, in the parameter plane (ρ, θ), the curve formed by the image points of the lines passing through P. If in the image there are several points aligned on the same line, in the plane of parameters, the curves that correspond to the transformations of the various points intersect at a point in the transformed plane that is the image of the line on which the points lie. Applying the Hough transform to an image one obtains an array containing all the lines found within the image. Finding the line with the minimum angle of rotation there is the certainty of finding the symmetry axis of the image.

2.3 Drill Bit Wear Estimation

The goal was to associate the image of a generic drill, on which there is no information, an indication on the number of holes that were made and on the number of holes that can still be carried out, so as to maximize the use of the single tip and avoid damage on the composite material processed. The proposed method and system associates each set of sixteen images with an array of values that identifies the surface profile of the two cutting edges with respect to the axis on which they are aligned. Each value of the output array gives a measure, in pixels, of the cutting edges' thickness while the number of elements in the array gives a measure of the length of the cutting edges. Seventy holes were made to age the drill bit and build on a carbon fibre laminate using a drill press. After every five holes, an image of the drill bit was acquired to check the degree of wear and observe any variations in the value of the average thickness, standard deviation, and integral profile. A picture of the used drill bit is reported in Figure 2.17, they have a diameter of 6 mm and are commonly used for aeronautical applications.

In Figure 2.18a, the profile of a new drill bit is reported, while in Figure 2.18b a comparison of the profiles of the same drill bit in different wear condition is reported; all the graphs refer to the same drill bit; only five profiles were

reported. The profiles were extracted with the previously described method.

A valley in the middle of the profile can be observed in both graphs; this coincides with the middle point of the drill bit. The adopted procedure allows the visualization of this deep, which can also be used as an indicator of the quality of the acquisition: in the case this feature is missing, the acquisition might be considered wrong. Symmetry in the two halves, with respect to the centre of the drill bit of the graph is also observable and repeatable among all the acquisitions in the different conditions. Depending on the nature of the analyzed drill bit, this symmetry could also be considered as a feature of the drill bit.

Comparing the profiles in the Figure 2.18b, even if the overall shape of the profile is maintained with the increase of the worn the drill bit, the drill bit' profile at different stages presents an average value that decreases with the

Figure 2.17: Drill bits used for the tests.
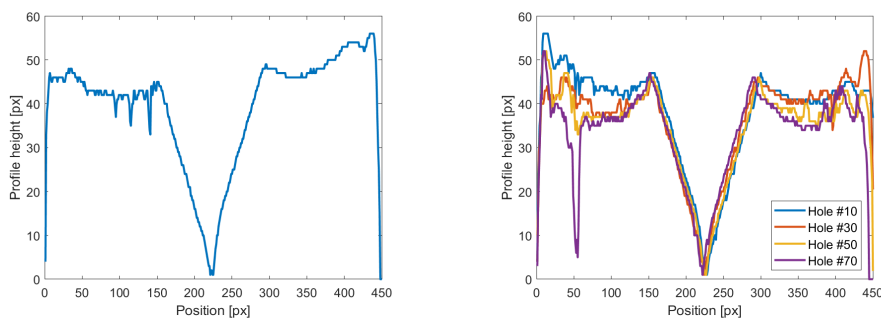
(a) The cutting edge profile extracted from a new and clean drill bit.

(b) Comparison of drill bit profiles with increasing wear level.

Figure 2.18: Drill bit profiles measured with the proposed method.

increase of the number of holes made with the drill bit. Moreover, a huge deep in the first half of the profile can be seen for the `Hole 70`; this particular case is due to a scratch on the surface caused by the drill bit wear; but in general this could also be caused by some particles attached to the surface of the drill bit tip that reflect the light in a different direction respect to the metal.

Acquisition	$< h >$ [px]	h Std. Dev. [px]	Σ [px]
1	38.4	12.0	17170
2	38.4	11.9	17228
3	38.5	11.9	17223
4	38.4	12.0	17163
5	38.3	12.0	17234
6	38.5	11.9	17223
7	38.4	12.8	17364
8	38.6	11.8	17312
9	38.8	12.4	17390
10	38.9	11.7	17266
Mean Value	38.52		17257
Std. Dev.	0.19 (0.5%)		76 (0.4%)

Table 2.1: Profile evaluation repeatability validation on a new and unused drill bit.

The repeatability of the profile extraction procedure was tested: in Table 2.1 the results of ten measurement on a new and unused drill bit are reported, each measurement was made by varying the position of the drill bit and re-capturing the images within the acquisition system. The illuminator was set to have two LEDs on (profile n. 3). Two synthetic parameters are reported in the table the $< h >$ value is the mean value of h calculated as in (2.3). The third column reports the standard deviation of h while Σ is the integral of the

profile height curve. For each value also the mean and the standard deviation are reported. As it can be seen from the table, the mean value of the new drill bit profile height is 38.5 px and its standard deviation is 0.19 px or less than the 0.5 %. Similar results (mean value of profile height and its standard deviation) were obtained for other drill bits of the same type and dimensions.

The measurement with the greatest sensitivity regarding the number of holes made is that of the average of the points of the zero derivative profile. The information to which this type of measurement refers is limited exclusively to the cutting edges' blades, which become thinner as the degree of wear of the tip increases. Measurements of the mean and integral of the algorithm's output array overall profile provide a more complete description of the cutting edge surfaces but have lower sensitivity as the remaining surface regions, such as the centre and corner edges of the cutting edges, during the drilling process they are not eroded as much as the blades.
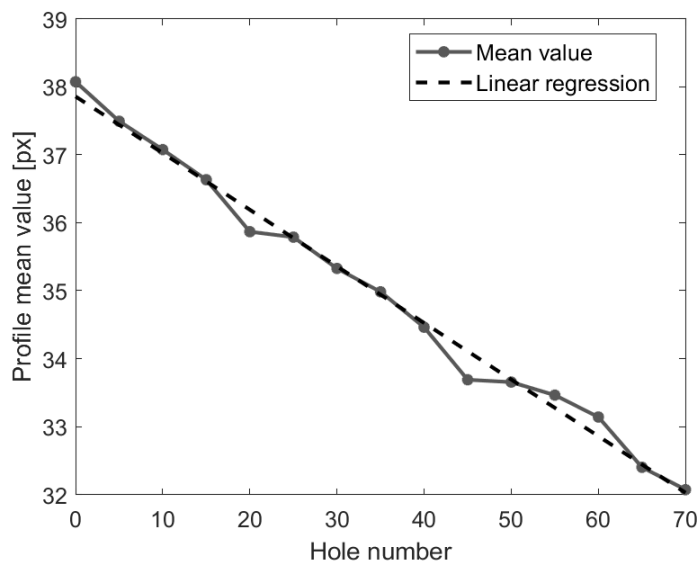
Figure 2.19: Mean value of the profile at varying number of hole and its linear regression.

Drill bits were aged and worn in a controlled environment using a column drill bit and a carbon fibre laminate, similar to the one used in the aeronautic industry to realize the fuselage. For every five holes made with the drill bit, the profile was analyzed several times and in different conditions. The graph in Figure 2.19 reports the mean value of the profile for a drill bit experimentally aged, the x-axis reports the number of holes made while the y-axis the mean value of the extracted profile ($< h >$) at the specific wear stage. A decreasing trend in the cutting edges' average thickness was observed as the number of holes increased.

The wear model that can be obtained with this method is expressed in equation (2.4), where $\hat{h}$ is the estimated hole number while m is the measured profile average value.

$$\hat{h} = \frac{m + 0.083}{37.85} \tag{2.4}$$

2.4   Conclusions

By comparing the profiles of the drill bit at different wear levels, a specific trend was found: the measured cutting edges' average thickness decreased as the number of holes increased. Considering this parameter, a linear wear model can be extracted from the measures and used as and indication of the residual life time of the tool. The information to which this type of measurement refers is limited exclusively to the cutting edges' blades, which become thinner as the degree of wear of the tip increases while Measurements of the mean and integral of the algorithm's output array overall profile provide a complete description of the cutting edge surfaces.

The presented method based on computational images can be used on tools with different blade shapes, and the linear regression of the average thickness is a first applicable approximation for a wear model. The use of visual inspection proves to be the quickest and most affordable method among the literature direct wear measurement method.

References

[AM03]   Issam Abu-Mahfouz. Drilling wear detection and classification using vibration signals and artificial neural network. *International Journal of Machine Tools and Manufacture*, 43(7):707 – 720, 2003.

[AUES06]   A. V. Atli, Oguzhan Urhan, Sarp Erturk, and M Sönmez. A computer vision-based fast approach to drilling tool condition monitoring. *Proceedings of The Institution of Mechanical Engineers Part B-journal of Engineering Manufacture - PROC INST MECH ENG B-J ENG MA*, 220:1409–1415, 09 2006.

[Can86]   J. Canny. A computational approach to edge detection. *IEEE Transactions on Pattern Analysis and Machine Intelligence*, PAMI-8(6):679–698, 1986.

[CAT17]   A. Caggiano, R. Angelone, and R. Teti. Image analysis for cfrp drilled hole quality assessment. *Procedia CIRP*, 62:440 – 445, 2017.

[DCS10]   Guifang Duan, Yen-Wei Chen, and Takeshi Sukegawa. Automatic optical flank wear measurement of microdrills using level set for cutting plane segmentation. *Machine Vision and Applications*, 21(5):667–676, Aug 2010.

[DPB$^+$16]   Joao A. Duro, Julian A. Padget, Chris R. Bowen, H. Alicia Kim, and Aydin Nassehi. Multi-sensor data fusion framework for cnc machining monitoring. *Mechanical Systems and Signal Processing*, 66-67:505 – 520, 2016.

[HSH19]   Qiulin Hou, Jie Sun, and Panling Huang. A novel algorithm for tool wear online inspection based on machine vision. *The International Journal of Advanced Manufacturing Technology*, 101(9):2415–2423, Apr 2019.

[JKK05] J. Jurkovic, M. Korosec, and J. Kopac. New approach in tool wear measuring technique using ccd vision system. *International Journal of Machine Tools and Manufacture*, 45(9):1023 – 1030, 2005.

[KB97] S. Kurada and C. Bradley. A review of machine vision sensors for tool condition monitoring. *Computers in Industry*, 34(1):55 – 72, 1997.

[KML+02] Jeon-Ha Kim, Deok-Kyu Moon, Deuk-Woo Lee, Jeong-suk Kim, Myung Chang Kang, and Kwang Kim. Tool wear measuring technique on the machine using ccd and exclusive jig. *Journal of Materials Processing Technology*, 130-131:668–674, 12 2002.

[LHvGVVV04] Cris Luengo Hendriks, Michael van Ginkel, Piet Verbeek, and Lucas Van Vliet. The generalized radon transform: Sampling, accuracy and memory considerations. *Pattern Recognition*, 38:2494–2505, 01 2004.

[MKJ00] M.A. Mannan, Ashraf A. Kassim, and Ma Jing. Application of image and sound analysis techniques to monitor the condition of cutting tools. *Pattern Recognition Letters*, 21(11):969 – 979, 2000.

[RB18] Raiminor Ramzi and Elmi Abu Bakar. Optical wear inspection of countersink drill bit for drilling operation in aircraft manufacturing and assembly industry: A method. *IOP Conference Series: Materials Science and Engineering*, 370:012041, may 2018.

[RJO05] Adam G. Rehorn, Jin Jiang, and Peter E. Orban. State-of-the-art methods and results in tool condition monitoring: a

review. *The International Journal of Advanced Manufacturing Technology*, 26(7):693–710, Oct 2005.

[vGLHVV04] Michael van Ginkel, Cris Luengo Hendriks, and Lucas Van Vliet. A short introduction to the radon and hough transforms and how they relate to each other. 03 2004.

[YON95] Yuchen Zhou, P. Orban, and S. Nikumb. Sensors for intelligent machining-a research and application survey. In *1995 IEEE International Conference on Systems, Man and Cybernetics. Intelligent Systems for the 21st Century*, volume 2, pages 1005–1010 vol.2, 1995.

[ZLYS06] W. J. Zhang, D. Li, F. Ye, and H. Sun. Automatic optical defect inspection and dimension measurement of drill bit. In *2006 International Conference on Mechatronics and Automation*, pages 95–100, 2006.

Chapter 3

Case Study: Water Leakage

The most important natural substance for the human being's life is clean water. Nevertheless, water leakage is widespread both in the distribution network for reason of obsolescence, corrosion, etc..., and at household level, after the meter, due to dripping taps, toilet cisterns faults, negligence, etc... In this chapter, after a brief introduction on the problem of water leakage and the methods traditionally used to check for leaks in piping systems, a technique for detecting leaks at home based on image analysis will be presented.

3.1 Introduction to Water Metering

The technical community has been urged to work to the former because it damages distribution companies, and numerous solutions have already been proposed [iURR15, WCOL15]. Until now, less importance or prominence has been given to the latter type of leakage because it is paid by consumers. In recent years, national and continental authorities have increasingly paid attention to problems concerning the resource monitoring aimed to avoid unnecessary waste and reduce consumption. This trend has extended the interest also to leakage after the meter. In a first study (1999) [MDF99] it was reported that in 1188 monitored houses, the average leakage ranged between 110.2 L/d (21.9 gphd, gallons per household per day), and about 342.2 L/d

(90.4 gphd) in about the 8.5% of the sample. The WRF's successive report
(2016) [DMDK16] provides an updated and expanded assessment of water use.
The report authors have identified some variations in water use, providing de-
tailed information and data on changes since the REU1999 study. The report
assesses a decline of about 22% respect to 1999 in water use across the resi-
dential sector, even as populations increase. In spite of use decrease, leakage
still amounts to 13% of indoor household water use, consisting in an average
absolute value of about 67.4 L/d (17.8 gphd).

3.1.1   Water Leakage

In a world where clean water is going to become an increasingly rare and pre-
cious good, no cause of waste is longer acceptable, regardless of the economic
interests that are affected. In support of this thesis, several scientific and
technical papers have been published in the last years that try to tackle the
problem of small water leakage detection at household level, but none of these
seem to be conclusive. In [SMC17], some consumption profiles concerning a
local small community network are reported. Data must be collected in a data
centre in order to detect suspect consumers and to conduct an audit to iden-
tify leakages. The water meter is an Arduino-based prototype that is very far
from series production, and no consideration of battery problems for domestic
application has been made even if three solutions for sending information to
the central data centre are proposed. Finally, no leakage detection algorithm
is proposed. A methodology for leakage detection at two scales (end-user and
District Metered Area) is reported in [SMC17]. Water smart meters are tra-
ditional water meters whose impulse sensor output is acquired by an impulse
sensor and transmitted via a radio frequency (169 MHz) to gateways. The
Advanced Metering Infrastructure, AMI, to get readings and detect leakage
was installed, as an experimental tested, at the University Campus. Neither
energy consumption nor transmission efficiency are evaluated. Smart meters
detect leakage and send alerts to the central unit by analysing the user con-

sumption profile. They based this approach on the analysis of hourly, daily, and seasonal variation in the consumption profile, including the evaluation of the minimum night flow. On this basis, meters send an alert when the leak probability exceeds a simple threshold: the average value plus two times the standard deviations.

More reliable seems the solution proposed in [FS17, FR18], where leakage detection relies on continuous off take monitoring and on setting daily limits. Continuous off take times are divided into time zones (for example, day/night), with single limits being entered either manually or based on, so-called, self-learning mode. Simulation tests seem to give encouraging results. However, the smart meter is made of an a.c. powered mini-PC connected to a pulse water meter. Consumptions are periodically transmitted to the cloud via an undefined wireless channel. Sithole at al. in [SRO+16] also propose a low-cost smart water meter prototype, based on a microcontroller (Arduino). It detects water leakage each time flow rate is constrained between 0 and 40 litres per hour for more than five seconds. Both the threshold and the time interval seem to be inadequate. In these last and some other contributes to the topic of small leakage detection at household level, two main lacks can be found: i) sensitivity of domestic water meters has not been considered at all; ii) smart meter communication capability must be mainly evaluated in terms of coverture range and battery life. The former lack affects the reliability of whatever leakage detection algorithm can be thought. All consumptions lower than the sensitivity of water meters cannot even be detected, let alone classified. The latter determines the viability of proposals. Smart water meters must be battery-powered devices that grant at least some years of battery life. Some studies on water consumption at household level agree considering that background leakage already occurs at 1 L/h flow rate and less, thus requiring meter sensitivity in the range of [0.1, 0.5] L/h to be detected. Based on the authors of [BSO13] instead, who studied the behaviour of over 22'000 households, the most common leakage rates are between 20 and 10 L/h, and

over 49% of leakages are 20 L/h. This last data would be comparable with the typical value of sensitivity of domestic water meters [20, 40] L/h, but lower values are still rare in commercial devices.

As for the smart meter communication capability, although still not so widespread, there are various types of smart meters that can either directly access to the Internet or connect to a gateway through short-range antennas. Whilst distribution network leakage detection algorithms always assume that measured data is processed centrally because they come from few big water meters that can be featured with big batteries, with regard to domestic consumption data should come with even greater continuity from many measurement points, one per user. These specifications generate bandwidth problems for short-range physical channels, and overload problems for GSM networks and server computers. In addition, the continuous transmission of rough data would be an additional load, hardly compatible with battery capacities that cannot exceed a few Ah. In 2018 the European Association of National Metrology Institutes (EURAMET), within the European Metrology Program for Innovation and Research (EMPIR), funded the Joint Research Project (JRP) "17IND13 Metrowamet – Metrology for real-world domestic water metering", that is aimed to study and to test smart metering solutions to solve the problem of leakage detection at household level. The authors are among the participants to the EMPIR JRP 17IND13 Metrowamet, thanks to their experience on wM-Bus at 169 MHz and on water smart meters [FMPP13, AGL+13, DLLP+16, CFP+17, FPP06]. In [ACLP19] the authors made a comparison between two domestic meters (an ultrasound digital flow meter and a multi-jet water meter) on the aptitude to measure small flows. In this paper, after a brief summary of the scientific literature in the field, they show the results of the tests they carried out to evaluate the water flow measurement sensitivity that can be achieved by featuring domestic analog water meters with a battery-powered processing and transmission unit.

3.1.2   Classical Water Leakage Detection Techniques

The classic method for detecting water leaks is the acoustic method, consisting
of techniques based on the relief of sound waves produced by water exiting a
break. These waves can be distinguished into two types:

1. waves that propagate longitudinally, along the pipe and the water column;

2. waves that propagate almost radially in the surrounding soil, starting from the point of leakage.

The characteristics of the sound wave and its propagation are influenced
by numerous factors such as water pressure, pipe material and diameter, the
nature of the soil and saturation conditions around the pipe, and the presence
of joints and discontinuities. Several tools have been developed to localize wa-
ter leakage that exploit the properties of sound waves generated by a rupture.
Classical acoustic instruments are the geophones used when noises are trans-
mitted from the ground, and the acoustic correlators, instruments measuring
the differences in the time of travel of the noise from the point of escape to
two sensors placed at the ends of the section of pipe under examination. With
such instruments, the pipeline route must be carefully traced until the leak is
located where the noise is generated.

Generally water leakage detection methods are divided into three cate-
gories [MIDAS$^+$19]: software based methods, hardware based methods and
conventional methods. In Table 3.1 a diagram of pipeline leakage detection
system divide into the three groups is reported.

Leak detection and location methods are based on pressure changes in the
water pipeline system; in general techniques for the detection of water losses
are:

- vibro-acoustic method: it foresees the use of instruments equipped with
  filters for the elimination of secondary noises (such as road traffic or

Pipe Leakage System	Software-based Methods	Hydrostatic Testing
		Mass Balance
		Pressure Point Analysis
		Statistical Analysis
		Multiple model Algorithm
	Conventional Methods	
	Hardware-based Methods	Tracer Gas Injection
		Infra-red Thermography
		Ground Penetrating Radar
		Acoustic Leak Detection
		Pipe Injection Gauge (PIG)
		Fibre-Optics Methods
		Vibration Methods
		Bi-wire Sensor

Table 3.1: Water pipeline leakage detection system methods divided into three groups.

other), able to pick up from the ground the noises and vibrations induced by the leak along the pipeline [LLM19]. An extensive review of vibration detection methods for water leakage can be found in [MIDAS$^+$19]. These methods are the most common because they are accurate, independent from the operator skill, and easy to use. Can be applied with ease on metallic piping but perform poorly on PVC [HCWG00, ABJ$^+$14] and large diameter pipe. Within this category vibrations can be measured in with two different sensors: piezoelectric sensors that present an analogue value to be acquired and process and the more common MEMES accelerometers that present a lower cost and higher sensitivity.

- Visual Observation and Optical method: when the pipeline is out of service or can be shut down for a few hours, it allows the possibility of carrying out, for diameters ranging from 100 to 2000 mm, an optical inspection by means of video inspection systems. Robotic inspection models with CCTV systems return the inspected route of the pipeline and its possible defects and damages. These video inspection operations can eventually be integrated with topographic surveys of the underground utilities [Zha97, ZT00]. These methods are able to detect leakage on pipeline systems and are also able to locate the leaks point but need experienced personnel and are time consuming.

- Method based on infrared thermography: it exploits anomalies in the radiation emitted by the surface of the ground, whose temperature is affected by the conditions produced by leaks and voids in the first section of the subsurface: this allows to highlight also anomalies in the conditions of laying of the pipeline. These methods measure the temperature gradient between the pipe and the soil [Jah18] resulting high sensitivity in detection of leakages.

- Method based on Ground Penetrating Radar (GPR): the saturation of the ground, caused by water, reduces the speed of the radar waves and

determines an image in which the pipe appears deeper than it really should be; the signal is partially reflected and picked up by a receiving antenna. The velocity of the wave depends on the dielectric constant at the surface of the pipeline. Different wave reflections are produced due to changes in the subsurface of the pipeline material [Lio98]. Radar signals are normally displayed vertically, so that a vertical section of the terrain is made. Ground Penetrating Radars are able to identify a leak on a pipeline and locate the leak point, on the other hand they are applicable only to non-metallic pipelines and need accurate selection of the inspection frequency depending on the soil nature, they require expensive equipment and trained operators because the results are difficult to interpret.

- Tracer Gas method: with this method, an area suspected of leaking is isolated, the pipe is emptied and then pressurized with a mixture of air and gas [HG98]. The most commonly used tracer gases are helium and hydrogen, both of which are non-toxic. Under pressure, the tracer gas escapes from the ruptures and rises to the surface, traversing the surrounding soil. Locating the leak is done by examining the soil surface with a portable gas sensor. The use of tracer gas is, however, very limited in water networks, due to the prior emptying to be carried out.

- Magnetic method: it uses an active system of RF localizers as well as a passive system of magnetic type. The RF locators work on appropriate detected frequencies [SRMJ15].

- Ultrasound system: it uses data processed by a measurement and detection system, able to sample the signals emitted by pipes subject to breakage and, subsequently, to make them available to operators by converting them into frequencies audible to the human ear.

- Laser Localization system: it allows, thanks to lasers equipment, to operate on the principle of detecting leaks by means of photo-acoustic

surveys.

A common aspect of all techniques that exploit sound waves is that they only allow the localization of water losses and not their estimation. Innovation in this field has been introduced by using devices (placed in opportunely chosen points of the water network) that are able to detect and transmit to a receiving unit a signal indicating alterations of the normal background noise conditions, thus adapting the acoustic signal to the surrounding environmental conditions. The innovative character of the method consists in operating continuously in a non-invasive way, carrying out monitoring activities with respect to the onset of new leaks, with a function of pre-localization, whose accuracy depends on the spatial density of the acoustic sensors and the technology used.

An application example is represented by a procedure developed for the first time in Great Britain, called PAC (Computerized Acoustic Pre-localization). This new technology allows a fast and economical automatic pre-localization of losses at night when network conditions are more favourable (low consumption, reduced noise due to withdrawals, less car traffic, less environmental disturbances, etc.). In this way, the use of qualified personnel takes place only in a subsequent phase aimed at localizing the leaks already pre-localized. The PAC system is based on the use of small electronic processors located in a network which, by means of an integrated system of measurement and analysis, allow to recognize the noises of the leaks from their sound level and download the data, through an interface, on a personal computer. The PACLOGs consist of a sensor to detect leaks, a data logger to store the data and a serial output for connection to the PC. These instruments should be placed inside wells on hydrants and valves, carefully recording the place and date of application of each PACLOG. Each PACLOG can cover, depending on the structure and network characteristics, a radius of about 150-300 meters. The PACLOGs are then automatically activated in the programmed periods (usually one or more analysis cycles between 1:00 and 4:00 am). The stretch in which the loss exists is identified and circumscribed with the help of the

(a) Installation at the "Laboratorio di In-
gegneria delle Acque" of "Università degli
Studi di Perugia".
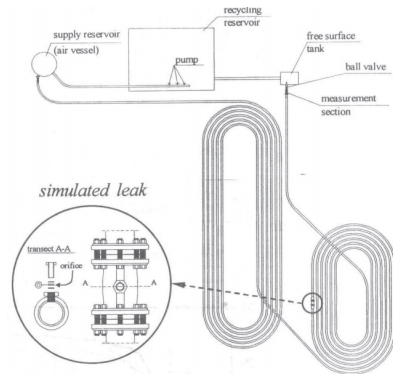
(b) Experimental layout and devices sim-
ulation the leak.   Image taken from
[BM01].

Figure 3.1: Installation and layout of the experimental setup in [BM01].

dislocation plan and according to the sound levels.

The method based on varied motion deserves particular attention. It in-
volves the survey of pressure waves generated by a transient of varied motion,
obviously of modest entity, to localize the rupture and estimate its entity,
exploiting the partial reflection elastic waves undergo in the presence of a
singularity [BM01]. This dual determination, combining estimation and lo-
calization of loss, gives this technique, which is in an advanced state of ex-
perimentation, considerable theoretical and applicative interest. The method
has been verified both by developing a numerical model and by considering
systems of different characteristics in the laboratory. In particular, the effects
on the response of the system have been investigated when the size and shape
of the leak change, as well as the conditions at its outlet

In Figure 3.1b a scheme of the used experimental installation, constituted
by a pipeline in PEbd (DN 110, thickness=8.1 mm, c 380 m/s velocity, length
352 m), equipped of a device for the simulation of the breakup (a trunk on
whose wall it possible to mount an orifice of variable form and dimensions) is
shown. In Figure 3.1a (1) is the tank with the pumps, (2) are the piping and
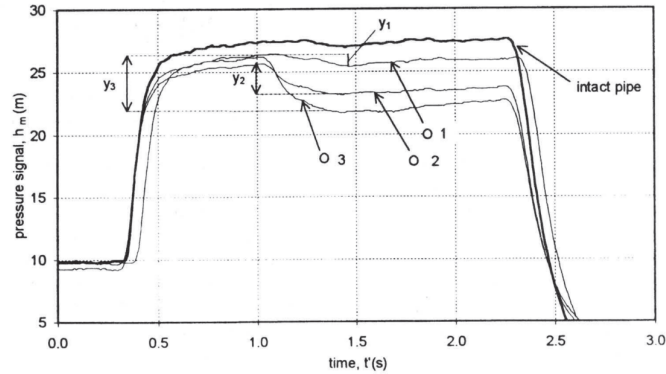
Figure 3.2: Pressure signal from intact and leaking pipe. Image taken from [BM01].

(3) is the end tank.

In Figure 3.2, the trend of the pressure transient determined by the abrupt closure of the end ball valve has been reported, detected in the section immediately behind the valve, both for intact pipeline and in case a leak is present (located at the $128.50\,\text{m}$ progressive). The tests indicated with 1, 2 and 3 in the figure correspond to gradually increasing dimensions of the orifice simulating the rupture (ratio Al/A between the section of the orifice and that of the pipeline equal, respectively, to 0.003, 0.011 and 0.029).

3.2 Image Analysis on Water Meters

Taking into consideration what the most common mechanical meter at household level are, an electronic add-on with a digital camera was applied on the top of the analog meters. The meter measures the water consumed by the customer and is interposed between the water distribution system and the customer's home appliances. For mechanical meters the black and white numbers on the dial show how much water you have used expressed in cubic meters. This is what companies uses to calculate the bill and what you should quote if they ask for a reading. On the same dial one or more needles is commonly

present, indicating the lower order water volume consumption. The add-on applied on the meter is able to take pictures of the meter and its digits with a colour camera. The classical image processing techniques are applied to the image to transform it in black and white and to obtain a binarized image.

The embedded measurement system based on image acquisition and processing was set up like in Figure 3.3b to capture data. It is featured with a camera with 480x640 resolution, and it is applied to the meter by means of a suitable case compliant with the glass displays of the meters. The main features of the electronic Add-On in Figure 3.3a is composed by:

- The camera module is an OV7670 provided by a low voltage CMOS image sensor. In a tiny footprint, it allows all the functionality of a single-chip image processor and VGA camera. The OV7670 makes available full-frame, sub-sampled, or windowed 8-bit pictures in different formats. The module is controlled via the Serial Camera Control Bus (SCCB) interface. The raw output image can be transferred to a suitable microcontroller using the Digital Camera Module Interface (DCMI). In addition, the consumption of the camera module is low: considering a 30 fps, its current consumption is less than 20 mA at 3 V in the active state and less than 100 µA in standby.

- The processing unit employed is a high-performance microcontroller STM32F4. It belongs to a microcontrollers' family based on the general-purpose ARM Cortex-M4. The STM32F4 is widely employed in many fields such as entertainment, power train, industrial automation, etc. In more detail, the microcontroller is based on a RISC core architecture at 32-bit operating up to 168 MHz. In addition, the Cortex M4 core implements full DSP set instructions and provides a Floating-Point Unit (FPU) single precision. The microcontroller offers, in addition, three 12-bit ADCs, two DACs, one SCCB, and one DCMI. Its memory features include a high-speed Flash memory RAM of up to 1 Mbyte and an SRAM of up to 192 Kbytes.

(a) Water meter Add-On.

(b) Experimental setup for meters characterizations.
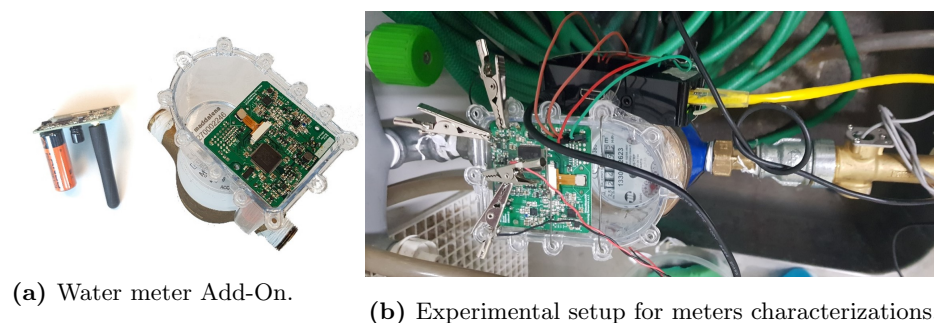
Figure 3.3: Embedded platform and experimental setup for meters characterizations.

- The hardware responsible for the low-range communication is in charge of the transceiver CC1120 manufactured by Texas Instruments, with the power front-end module SKY65367-11 manufactured by SKYWORKS. The CC1120 transceiver conforms with EN 13757-4:2013 standard, regulating in a short-range network the WM-Bus operation. In more detail, the prototype has been set up to operate at maximum transfer power in N2a mode. In addition, the SKY65367-11 has been adapted to enhance the power provided to the antenna at up to 27 dBm.

- The smart add-on is battery-powered, utilizing two low discharge lithium batteries with a total capacity of 7000 mAh (3.6 V).

Three water meters, all compliant with Directive 2014/32/EU (Annex MI-001), were chosen to experimentally test the effective sensitivity to very small flow rates. The first water meter is a dry dial multi-jet water meter (Figure 3.5a), the second is a flow-through ultrasonic meter, while the third is a dry dial volumetric rotary piston water meter (Figure 3.5b).

The main steps of the processing procedure are:

- First, the consumption indicator of a mechanical meter crossed by four different hourly flow rates (0 l/h, 8 l/h, 12 l/h and 20 l/h) was monitored for an extensive period of time. A camera mounted on a support integral

with the meter took photographs, with a period of one second, of the dial of the meter throughout the process; from each of these photos the region of interest (ROI) was cut; in this case the ROI corresponds to the dial that indicates consumption, an example of the ROIs is reported in Figure 3.4, where two different indication types are reported: a needle (Figure 3.4a) and a rolling digit (Figure 3.4b).

- Subsequently, the ROIs relative to the four different consumption profiles have been elaborated. For each of the four considered flow rates, the difference in modulus between an ROI and the succesive one has been calculated. The two ROIs are distant each other a sampling period T. By making the difference between two ROIs it is possible to observe approximately the derivative of the consumption trend.
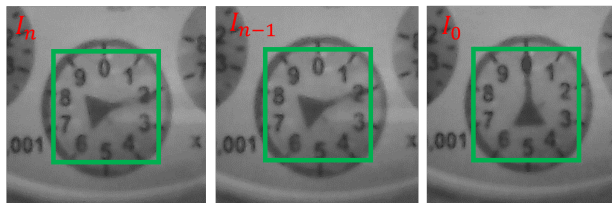
(a) Region of Interest for a Multijet water meter with needle indicator.
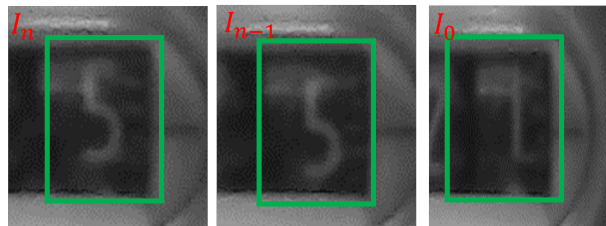
**(b)** Region of Interest for a volumetric water meter with digit indicator.

Figure 3.4: Region of Interest (ROI) for two different analog water meter with different technology indicators. Here are reported three different samples of the same indicator.

The two analog water meters have a mechanical display whose readability is guaranteed by a mineral tempered glass lens, with five digits in the multi-jet,
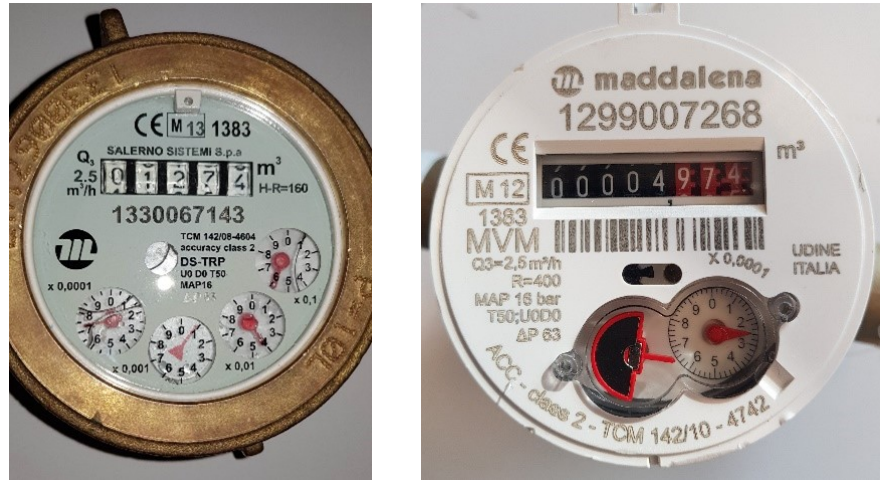
(a) Multi-jet water meter.

(b) Volumetric rotatory piston water meter.

Figure 3.5: The analyzed analogic water meters.

whilst eight digits in the piston. The metrological performance of the mechanical meters is fully described on their manufacturer (Maddalena) data-sheet. The ultrasonic sensor is conditioned by a digital circuit that continuously (not faster than 1 Hz) provides the flow rate [L/h] value. A microcontroller-based interface downloads measurement data via serial port at 4800 bit/s. An internal electronic accumulator provides the total amount of m3 of water from the last reset.

The performances of the ultrasonic meter was obtained by a characterization procedure, carried out at the "LAMI" Laboratory of the University of "Cassino and southern Lazio", where the ultrasonic sensor was included in a loop together with a constant flow rate generator, as it can be seen in Figure 3.6a. The experimental results of the characterization are reported in Figure 3.6b and are fully compliant with EU Directives.

(a) The characterization station of the "LAMI" Laboratory.
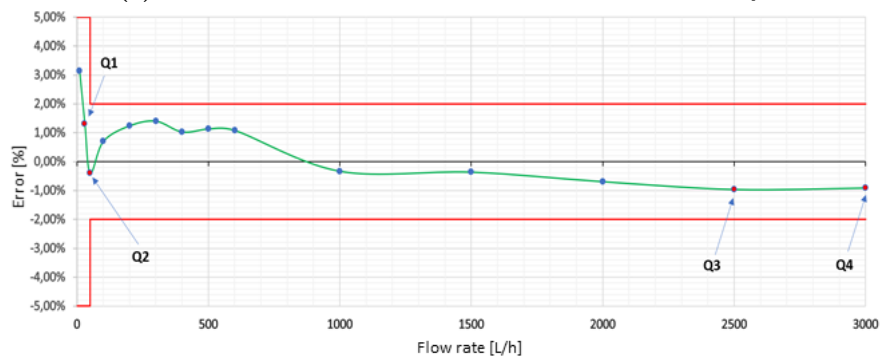
(b) Experimental results of the ultrasonic sensor hydraulic characterization.

Figure 3.6: Experimental characterization station and results for an ultrasonic sensor.

3.2.1 Cross-Correlation Experimental Results

The images acquired by the camera are processed to monitor the consumption and, overall, to detect small leakage, characterized by the absence of a period with null consumption. Therefore, the image processing software aims to monitor the counter's display changes or, in other words, analyse the similarity/dissimilarity between successive images of the counter.

Different approaches can be used to measure the similarity/dissimilarity between images, such as Cross-Correlation, Euclidean Distance, Manhattan Distance, and many others. However, Cross-Correlation is used in many applications thanks to its non-polarized estimate.

In [CIDL$^+$20] a cross-correlation based approach to the similarity detection in image processing Figure 3.7:

$$r(I_A, I_B) = \frac{\sum_j \sum_i (I_A(i,j) - \bar{I}_A) \cdot (I_B(i,j) - \bar{I}_B)}{\sqrt{\sum_j \sum_i (I_A(i,j) - \bar{I}_A)^2} \cdot \sqrt{\sum_j \sum_i (I_B(i,j) - \bar{I}_B)^2}}, \quad (3.1)$$

where r is the cross-correlation index, I_A and I_B are the two images to be analysed, $I_x(i,j)$ are the pixel values of the generic image, and $\bar{I}_x$ is the mean value of the image. The cross correlation value is $-1 \leq r(I_B, I_B) \leq 1$.

Using cross correlation (3.1) it is possible to detect small water leakages on mechanical water meter even in case of dynamic conditions, like when digits turn in their register due to the measurand. In Figure 3.7 an example of cross-correlation applied to the digits of the analogic water meter is reported. With reference to Figure 3.7 the cross-correlation values are the following:

- $r(I_A, I_A) = 1$ the two analyzed images are identical,

- $r(I_B, I_B) = -1$ the image I_B has been generated as the inverse of I_A,

- $r(I_C, I_C) \geq 0.07$ the two images are uncorrelated.

It is easy to demonstrate that if the digits rotate with constant speed, the cross-correlation versus time tends to a periodic waveform. The variability of
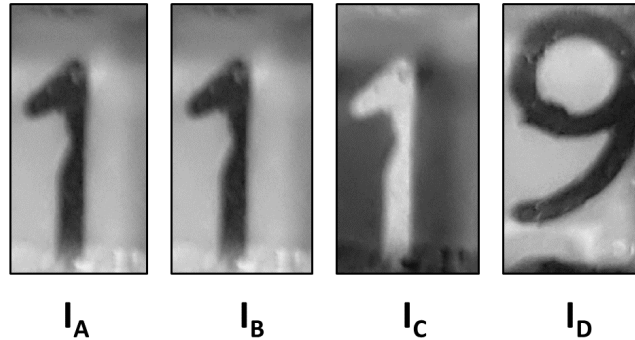
Figure 3.7: Images of a register submitted to cross-correlation

the 2D cross-correlation factor due to small changes in a couple of correlated images was significant and repetitive enough to be used for discriminating the similarity from dissimilarity with good sensitivity. This approach showed to be particularly effective in detecting changes in mechanical meter registers.

Several experiments were carried out in a test bed where any type of domestic water meter could be included in a loop where water can flow at any fixed constant flow rate. The experimental results of tests carried out on two different types of indicators (needle and digit) that can be found in meter registers were encouraging and let suppose that this approach can also be considered a starting point towards the definition of metrics for small water leakage detection. Future efforts will be driven to the definition and characterization of these metrics, and the development of suitable leakage detection algorithms based on image processing.

In Figure 3.8 the cross correlation factor versus time in dynamic condition is reported with different flow rates: 0.8 L/h, 1.6 L/h, 2.4 L/h and 3.2 L/h. As it can be seen the resulting waveforms seems to be periodic, and peaks correspond to the maximum similarity of the $n-th$ image with the first taken image in the same dial condition. In dynamic conditions (non-zero flow), this happens at each complete turn of the digit. From this consideration, it is possible to say that the time between two consecutive peaks is the time necessary to a water volume V in litres to flow through the meter; and the
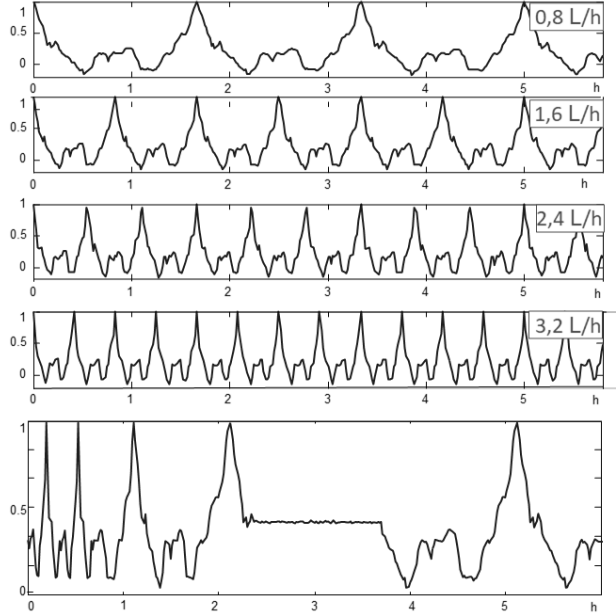
Figure 3.8: Cross-correlation factor versus time in dynamic conditions.

water volume is given by:

$$V = 10 * \text{Resolution.} \tag{3.2}$$

In this case, measuring the peak distance on the time axis (Δt [h]), a rough measurement of the flow rate can be obtained as flow rate (ϕ [L/h]) is proportional to the resolution divided by the time interval (Δt):

$$\phi = 60 * 10 * \frac{\text{Resolution}}{\Delta t}. \tag{3.3}$$

It's important to note that aliasing arises at flow rates higher than the frame-rate (N_{frames}/h) multiplied by ten time the resolution.

$$\phi \leq N_{\text{frames}}/h * 10 * \text{Resolution} \tag{3.4}$$

With reference to the last graph in Figure 3.8 in the presence of a variable flow, a period of about 100 minutes of zero flow rate can be easily detected

in part were the correlation factor keeps constant. It appears clear that the cross-correlation factor could be a good starting point to define metrics which a small leakage detection algorithm could be based on.

3.2.2   Cross-Correlation Reset Strategy

In order to evaluate the generality of the image similarity detection approach, two different types of mechanical water meters were tested on the same test rig. The mechanical water meters utilized belong to the two most widespread types of domestic water meter: multi-jet and volumetric (piston). Both measure the total volume of cold water flowed through them since reset. While the former is one of the most commonly used water meters at the household level due to the operational simplicity and low cost, the latter assures higher accuracy and sensitivity at low flow rates. In multi-jet water meters, the principle of operation is based on the passage of the inlet water flow through ducts open in a chamber containing the turbine. The water through the ducts generates symmetrical water jets that impact the turbine keeping it in a perfect balance. The rotation of the latter acts the reading mechanism enabling the measurement of the water volume passing through the meter. The turbine speed is proportional to the water flow in the inlet. The used dry multi-jet water meter has 5 digits and 4 needles, the last significant digit corresponds to 1 m3, whilst the last needle indicates with $0.0001\,\mathrm{m}^3$ of resolution.

The operation principle of a volumetric water meter is based on a piston rotating within a chamber of specific volume. Each rotation will allow an amount of water to pass through the piston chamber. The used volumetric water meter has 8 digits and 1 needle; the last significant digit corresponds to $0.001\,\mathrm{m}^3$, whilst the last needle indicates with $0.0001\,\mathrm{m}^3$ of resolution.

Both meters were featured with the electronic add-on device whose frame rate was fixed at 60 frames/h. The image similarity detection approach was applied to the 0.001 m3 needle of the multi-jet and the last digit $(0.001\,\mathrm{m}^3)$ of the piston. At each $n - th$ new frame acquisition (I_n), two different cross-
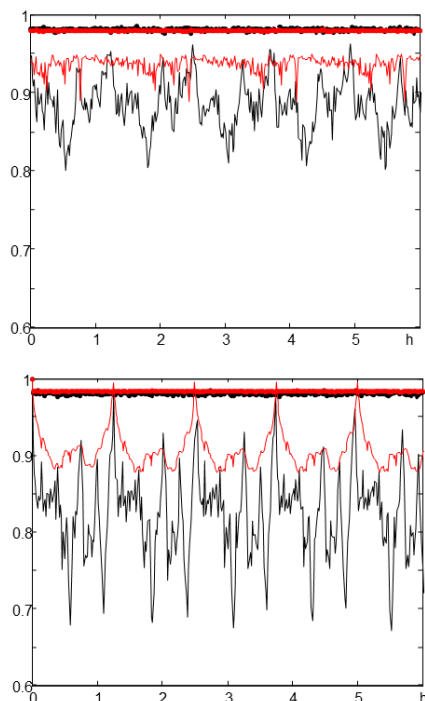
Figure 3.9: Measured cross-correlation coefficients r_d and r_0 for two different flows (points with 0 L/h, line with 8 L/h) in a time window of 6 hours of both the water meter considered.

correlation factors were calculated:

$$r_d(n) = r(I_n, I_{(n-1)}),\qquad\qquad\qquad\qquad (3.5)$$

$$r_0(n) = r(I_n, I_0).\qquad\qquad\qquad\qquad (3.6)$$

Where I_0 is the image acquired at the beginning of the procedure.

In Figure 3.9 a couple of measured cross-correlation coefficients is reported. Tests were 6 hours long, and some statistics on rd for both meters are reported in Table 3.2, while both the cross-correlation factors (r_d and r_0) at two flow rates (0 L/h and 8 L/h) are reported versus time for the volumetric meter and, for the multi-jet. Looking at Table 3.2, where the average value μ of r_d was calculated on a 20 point sliding window together with the related standard

Meter	Volumetric		Multi-jet	
Flow Rate [L/h]	μ	σ	μ	σ
0.0	0.980	0.002	0.9878	0.0004
4.0	0.924	0.034	0.9461	0.0085
8.0	0.833	0.048	0.895	0.012
20.0	0.785	0.061	0.832	0.033

Table 3.2: Statistics of measured cross correlation parameter r_d at different flow rates.

deviation σ, the first considerations to do are: similarity corresponds to null flow rate and is characterized for both meter registers by high μ and very low σ. As for non-zero conditions, the dissimilarity is clearly detectable: the more the flow rate, the more the σ value and the less the μ value.

## 3.2.3   Period with Null Consumption Monitoring

The main part of the literature about water leakage detection focuses on comparing consumption thresholds in terms of flow rate [L/h]. While this approach is fully compatible with the static flow meters, it does not fit entirely with volumetric mechanical meters, measuring volume [m^3]. The continuous off take and the Period with Null Consumption (PWNC) monitoring represent a practical approach to developing a robust method for detecting small leakages. More in detail, both quantities are time interval values characterized respectively by the non-zero or null value of measured flow [L/s]. In the absence of leaks, the offset can be continuous only for a limited time interval (a threshold); the presence of water leakage can be detected if a continuous offset overcomes this threshold. Threshold, to be effective, must be chosen differently by day and night: while maximum off take occurs during daily hours, no considerable long-term offtake is expected during the nightly hours requiring a threshold consistently lower. If there is no leakage downstream of the

meter, several PWNCs should appear for an entire day. On this basis, leakage detection can be made from continuous monitoring of off take by algorithms that could be implemented on smart meters and central units. In both cases, meter sensitivity (the minimum value of flow rate able to provide a change in the meter display) determines the minimum leakage that any algorithm will be able to detect. On the other hand, this intrinsic limit of meters also represents the minimum flow rates that can increase the measured customer consumption and consequently its bill.

According to the PWNC algorithm, an absence of leakage can be assumed when no changes are seen in the water consumption measured by the water meter according to its metrological characteristics (e.g., starting flow rate, range, sensitivity). However, due to the most common water meter's mechanical characteristics adopted in the domestic scenario, a different approach can be pursued for discovering a water leakage. Indeed, these meters characterized by mechanical elements as turbine, or piston, if subjected to a long period under a small water flow (smaller than the starting flow rate), will reveal an intermittent movement of the needle. This fact is caused by the accumulated quantity of water, which will cause an inertial force to run for an instant the main shaft of the water meter. The use of a PWNC algorithm based on the correlation among two consecutive meter display images allows discovering, using the principle described above, the detection of leakage under the water meter starting flow rate improving as a consequence, the sensitivity of mechanical registers concerning the leakage phenomena. Indeed, the leakage's sensitivity corresponds to the water meter sensitivity for all the existing water leakage devices and technology under research.

The idea beyond leakage detection is to find metrics sensible to the previously described phenomena (intermitting operation of the water meter under the starting flow rate) to improve the whole meter's sensitivity. In this regard several experimental tests were made first with constant flow rates and then with dynamic water consumption profiles.
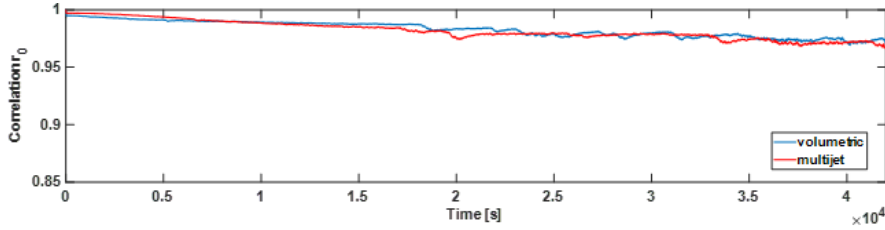
Figure 3.10: Cross-correlation coefficient r_0 with null flow rate condition for volumetric and multi-jet water meter.

The previously proposed r_0 index (correlation index between the actual image and the reference one) has been calculated for the water meters considering a null flow rate. This test has led to evaluating the r_0 variability, over an extended observation window, due to everyday external events such as the daily external light changing or random vibrations. In Figure 3.10 have been reported correlations r_0 calculated on the ROIs containing the needles when a null flow is applied for 12 hours. As can be seen over all the periods, the correlations r_0 fall into a slight interval for both meters, respectively 0.997 to 0.967 for the multi-jet and 0.995 to 0.969 for the volumetric. Then, the same index r_0 has been calculated considering a flow rate of 1 L/h for the multi-jet water meter (lower than its starting flow rate).

The calculation of r_0 has revealed to be a valuable metric to be considered for leakage detection purposes. However, the only observation of instantaneous values of r_0 could not be sufficient to provide a reliable leakage indication since unexpected external influences such as shock or knock could influence its value. This is demonstrated in Figure 3.11a, where around the fifth hour of the test, the accumulated quantity of water has provided a drop of the correlation r_0, revealing the intermittent movement of the needle. An effective parameter that should be immune from these issues mentioned; this parameter could be the standard deviation of the r_0 over a sliding window (σ_{r_0}). The window length selection must be made considering the trade-off between a too-small window that could lead to false detection and a too-long window presenting
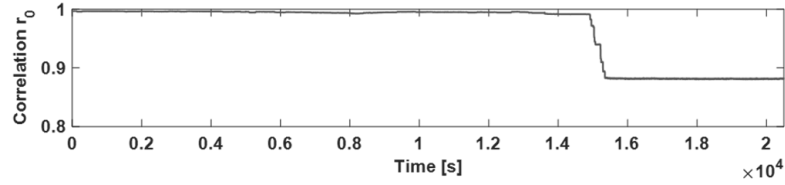
(a) Evolution of r_0 for a flow rate of 1 L/h.
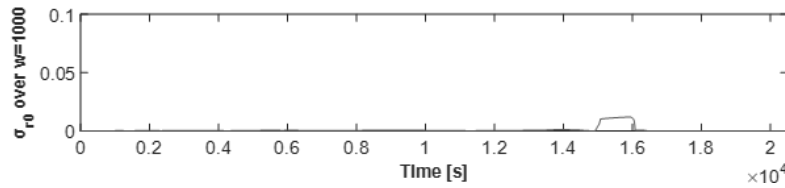
(b) Evolution of σ_{r_0} for a flow rate of 1 L/h.
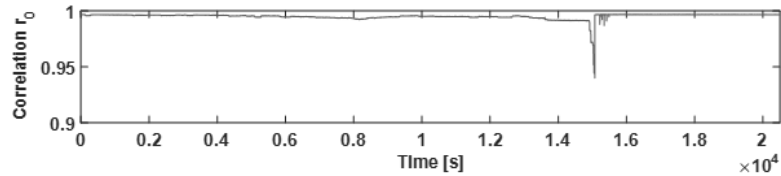
(c) Evolution of r_0 for a flow rate of 1 L/h with the reset strategy enabled.

Figure 3.11: Comparison of the evolution of r_0 for a flow rate of 1 L/h with and without the reset strategy for the volumetric meter.

lower sensitivity to the phenomena under observation missing the detection. A window equal to 1000 samples revealed to show the best performance, showing an adequate sensitivity according to the phenomena under observation: intermittent operation after a long observation.

It has to be pointed out that, because of intermitting operation or normal consumption, the actual acquired image can change significantly from the reference image, I_0, and consequently, r_0 decreases or increases, reducing the sensitivity to very low consumption. This problem can be handled by replacing the reference image I_0 with the current image I_n after detecting a consumption as can be seen in Figure 3.11c, where compared to Figure 3.11a, after the intermitting phenomena, the correlation r_0 will fall back to the highest value representing a null flow rate condition. Figure 3.11b reports the σ_{r_0} calculation

for the static profile test of 1L/h. As it can be seen, the σ_{r_0} can highlight even better the dropping event. For this reason, the evaluation of the standard deviation σ_{r_0} over a sliding window has been revealed to be a metric showing an adequate sensitivity to the leakage detection aim.

This analysis shows that, by comparing r_0 and σ_{r_0} with suitable thresholds, a PWNC can be identified. Generally, it can be affirmed that the r_0 values decrease and the σ_{r_0} over the sliding window increase significantly for the three-profile starting the observation from the zero flow rate to their relative starting flow rate. Threshold values for r_0 and σ_{r_0} can be experimentally evaluated and used as for a PWNC identification: it can be made by comparing new calculated indexes with the threshold values.

3.3   Conclusions

Pipeline networks are essential for transporting water from one destination to another, but a large percentage of water is lost in transit from the treatment plant to the consumer. Water leakage represents an important issue, particularly in developing countries, both economically and in terms of precious natural resources. Leak causes are various: they may occur due to ageing pipelines, corrosion, and excessive pressure resulting from operational error and valves' rapid closing or opening. In order to detect water leakages and the size of a leakage, many techniques have been proposed in the literature.

Classical approaches use acoustic measurement with different analysis methodologies with various types of computer software to analyze the measured data from internal pipeline parameters, such as pressure, flow rate and temperature. They also make use of experienced personal walking along the pipeline with complex instrumentation.

The use of visual inspection on piping networks is not new, but it has been applied to the inspection of the piping or of the thermography images of the soil. The here presented use of image analysis at the customer level allows

the water company to equip existing water metering appliances with a custom add-on capable of detecting water leakage at the household level.

Cross-correlation reveals to be an effective method for the detection of changes in mechanical registers, showing a high independence from the indication technology of the meter. It does not need any a-priori template to work correctly, meaning that very little work is needed by the operator or the water company interested in using this type of analysis to reduce the water leakage detection at the household level. Cross-correlation achieved a high degree of repeatability; the two parameters give different indications: r_d gives more chance to have a sudden and accurate detection of both similarity ad dissimilarity meanwhile r_0 allows a rough estimate of the flow rate, with higher accuracy of the needle than the digit resulting in a fast detection of a small leakage. On the other hand no reference curve can be defined to allow water leakage detection but parameters like "Continuous off take" and "Period With Null Consumption" can be monitored with adequate sampling time.

References

[ABJ+14] Fabricio Almeida, Michael Brennan, Phillip Joseph, Stuart Whitfield, Simon Dray, and Amarildo Paschoalini. On the acoustic filtering of the pipe and sensor in a buried plastic water pipe and its effect on leak detection: An experimental investigation. *Sensors (Basel, Switzerland)*, 14:5595–610, 03 2014.

[ACLP19] Francesco Abate, Marco Carratù, Consolatina Liguori, and Antonio Pietrosanto. Smart meters and water leakage detection: a preliminary study. 05 2019.

[AGL+13] Alfonso Attianese, Antonio Giudice, Marco Landi, Vincenzo Paciello, and G. Graditi. Synchronization of dlms/cosem sensor nodes. 07 2013.

[BM01] Brunone Bruno and Ferrante Marco. Detecting leaks in pressurised pipes by means of transients. *Journal of Hydraulic Research*, 39(5):539–547, 2001.

[BSO13] Tracy Britton, Rodney Stewart, and Kelvin O'Halloran. Smart metering: Enabler for rapid and effective post meter leakage identification and water loss management. *Journal of Cleaner Production*, 54:166–176, 09 2013.

[CFP+17] Marco Carratù, Matteo Ferro, Vincenzo Paciello, Antonio Pietrosanto, and P. Sommella. Performance analysis of wm-bus networks for smart metering. *IEEE Sensors Journal*, 17:7849–7856, 08 2017.

[CIDL+20] Marco Carratù, Salvatore Dello Iacono, Giuseppe Di Leo, Consolatina Liguori, and Antonio Pietrosanto. Image based similarity detection in mechanical registers. In *2020 IEEE International Instrumentation and Measurement Technology Conference (I2MTC)*, pages 1–6, 2020.

[DLLP+16] Giuseppe DI Leo, Consolatina Liguori, Vincenzo Paciello, Antonio Pietrosanto, and P. Sommella. *Smart Meters in Smart Cities: An Application of DLMS-COSEM on 169 MHz WM-Bus*, pages 735–746. 01 2016.

[DMDK16] W.B. DeOreo, P.W. Mayer, B. Dziegielwski, and J.C. Kiefer. *Residential Uses of Water 2016*. Water Research Foundation, Denver, CO, 2016.

[FMPP13] L. Ferrigno, R. Morello, V. Paciello, and A. Pietrosanto. Remote metering in public networks. In *Metrology and Measurement Systems*, volume 20, pages 705–714, 2013.

[FPP06] Luigi Ferrigno, Antonio Pietrosanto, and Vincenzo Paciello. Low-cost visual sensor node for bluetooth-based measurement networks. *Instrumentation and Measurement, IEEE Transactions on*, 55:521 – 527, 05 2006.

[FR18] Jan Fikejz and Jiři Roleček. Proposal of a smart water meter for detecting sudden water leakage. In *2018 ELEKTRO*, pages 1–4, 2018.

[FS17] Elias Farah and Isam Shahrour. Smart water for leakage detection: Feedback about the use of automated meter reading technology. In *2017 Sensors Networks Smart and Emerging Technologies (SENSET)*, pages 1–4, 2017.

[HCWG00] Osama Hunaidi, Wing Chu, Alex Wang, and Wei Guan. Detecting leaks in plastic pipes. *Journal AWWA*, 92(2):82–94, 2000.

[HG98] Osama Hunaidi and Peter Giamou. Ground-penetrating radar for detection of leaks in buried plastic water distribution pipes. 1998.

[iURR15] Nataša S. Živic, Obaid Ur-Rehman, and Christoph Ruland. Evolution of smart metering systems. In *2015 23rd Telecommunications Forum Telfor (TELFOR)*, pages 635–638, 2015.

[Jah18] Sebastian Ingo Jahnke. Pipeline leak detection using in-situ soil temperature and strain measurements. 2018.

[Lio98] Chyr Pyng Liou. Pipeline leak detection by impulse response extraction. *Journal of Fluids Engineering-transactions of The Asme*, 120:833–838, 1998.

[LLM19] Amartansh , Zhao Li, Pedro Lee, and Ross Murch. Measurement and characterization of acoustic noise in water pipeline channels. *IEEE Access*, 7:56890–56903, 2019.

[MDF99] P.W. Mayer, W.B. DeOreo, and AWWA Research Foundation. *Residential End Uses of Water*. AWWA Research Foundation and American Water Works Association, 1999.

[MIDAS+19] Mohd Ismifaizul Mohd Ismail, Rudzidatul Akmam Dziyauddin, Noor Azurati Ahmad Salleh, Firdaus Muhammad-Sukki, Nurul Aini Bani, Mohd Azri Mohd Izhar, and L. A. Latiff. A review of vibration detection methods using accelerometer sensors for water pipeline leakage. *IEEE Access*, 7:51965–51981, 2019.

[SMC17] M. Suresh, U. Muthukumar, and Jacob Chandapillai. A novel smart water-meter based on iot and smartphone app for city distribution management. In *2017 IEEE Region 10 Symposium (TENSYMP)*, pages 1–5, 2017.

[SRMJ15] W. Sharatchandra Singh, B. Purna Chandra Rao, Chandan Kumar Mukhopadhyay, and T. Jayakumar. Detection of localized damage in water wall tubes of thermal power plants using gmr sensor array based magnetic flux leakage technique. *Journal of Nondestructive Evaluation*, 34:1–7, 2015.

[SRO⁺16] Bheki Sithole, Suvendi Rimer, Khmaies Ouahada, C. Mikeka, and J. Pinifolo. Smart water leakage detection and metering device. In *2016 IST-Africa Week Conference*, pages 1–9, 2016.

[WCOL15] Jin Wang, Rachel Cardell-Oliver, and Wei Liu. Discovering routine behaviours in smart water meter data. In *2015 IEEE Tenth International Conference on Intelligent Sensors, Sensor Networks and Information Processing (ISSNIP)*, pages 1–6, 2015.

[Zha97] Jun Zhang. Designing a cost-effective and reliable pipeline leak-detection system. *Pipes & pipelines international*, 42:20–26, 1997.

[ZT00] Jun Zhang and Michael Twomey. Statistical pipeline leak detection techniques for all operating conditions. 229, 01 2000.

Chapter 4

Case Study: Beer Colour Analysis

Small industrial realities are increasingly common and are developing in every country. The demand for low-cost solutions that could be adopted where the staff is not highly qualified or where the budget is growing. An example is microbreweries, where it is necessary to control the quality and characteristics of the product to ensure its reproducibility.

In this chapter, image analysis is reduced to the analysis of a single colour point in order to identify a parameter known as EBC. After a brief discussion of the problem and the qualitative properties of beer, a low-cost solution is analysed to measure the EBC of a beer.

4.1 Introduction to Beer Production and Microbreweries

Nowadays, beer has entered the customs and traditions of almost every country globally that produce and consume it. Beer cannot be considered simply as an alcoholic beverage: it has essential nutritional properties; in general, it contains less ethanol ethanol than any other alcoholic beverage, and it can be

considered as authentic and proper food. The brewing industry has become a business of global proportions, and every year several tens of billions of litres of beer are consumed, with several turnovers of hundreds of billions of dollars. The industrial beer producers are constituted by few companies around which coexist many thousands of smaller producers.

In recent years, the production of craft beer has been constantly increasing with the establishment of hundreds of microbreweries producing a variety of beer types with different sensory characteristics that make them attractive compared to the industrial production [Bee]. To maintain an adequate quality standard, microbreweries need quality control systems for the product and the production process as well as the industrial breweries. Craft beer production is often made by small enterprises that cannot afford the cost of the quality control systems used by industrial breweries, so they require low-cost solutions in order to guarantee a fulfilling quality. Although they produce a handmade product, the quality requirements are the same as for the industrial breweries, but often the cost to equip a quality laboratory cannot be supported, due to their limited financial capabilities. To overcome this problem, craft breweries need low cost instruments in order to check the main quality parameters like colour, which is usually used to verify both the process and the product quality.

Beer is one of the oldest and widespread alcoholic beverage in the world. It is obtained from the brewing process of malt, water, hop and yeast. A variety of styles can be obtained using a blend of different kinds of malt and hop, characterized by several physical and sensory properties like alcohol content, bitterness, colour, pH, body and foam stability [Meu09, LDR$^+$15]. The beer quality parameters are measured according to standard analytical methods that have been worldwide adopted by the industrial breweries in their quality control laboratories [Con07, oAB09]. The quality control procedures often require expensive instruments and skilled personnel, so the cost to equip a chemical laboratory is not affordable by the smallest companies, like microbreweries. Microbreweries are craft beer producers with a limited annual

production fixed by law, allowing to obtain a product of higher quality superior to beers produced at an industrial level. According to the statistics report of the "The brewers of Europe" association, the number of microbreweries in Italy increased from 407 in 2012 to 692 in 2018, and they represent about the 80 % of the active breweries [Bee]. Most of these companies are small enterprises, with reduced financial capacity, that are not able to invest in expensive laboratory instrumentation. Nevertheless, the microbreweries need to evaluate the main quality parameters of their products, so they look for cheaper methods to determine the characteristics of the beer.

For example, the alcohol content is often estimated using an indirect measurement of density that can be made with cheaper instruments and easier than the direct measurement employing distillation, gas chromatography or refractometry as requested by the international standard methods. The indirect method is based on the relation between the alcohol content by volume and two densities, the Original Gravity (OG) and Apparent Gravity (AG), which represent, respectively, the relative density, compared to water, of the beer wort before and after the fermentation [CRS09]. This method, although cannot be compared to the official procedures, allows having a good estimation of the alcohol content. Computer vision methods have been also proposed in order to evaluate the quality attributes of the beer related to the visual appearance, like colour, foam stability, bubble size distribution [LMM+19]. These methods allow performing automatic inspection with fast and objective results respect to the manual inspection, but particular attention must be paid to the illumination condition strongly affecting the performance of the vision systems, especially for the colour evaluation. Regarding the sensory attributes, the use of electronic noses has been explored for the classification of the ingredients and the defects, like the presence of off-flavors [SLA17, GVMRM+11].

Another important parameter in beer production is the pH value. Measurement of pH plays a crucial role in a wide variety of applications, such as food and beverage, pharmaceutical industry, water treatment, biology, medicine.

pH measures the acidity or alkalinity of aqueous solutions. It is a dimensionless quantity defined as the negative logarithm of the activity of hydrogen ions in an aqueous solution at a given temperature [YJK05]. In particular, in neutral solutions there is an equilibrium between hydrogen ions (H+) and hydroxyl ions (OH-), the relative number of hydrogen ions is higher than hydroxyl ions in acidic solutions, while it is lower in alkaline solutions [YJK05, ZSI$^+$15]. The typical range of pH values is from 1 to 14, where 7 indicates a neutral solution, a greater value indicates a more alkaline solution, while a lower value indicates a more acidic solution. The methods for pH measurement are mainly divided in: electrochemical and optical.

Electrochemical methods are based on electrodes that transduce the chemical activity of the hydrogen ion into an electronic signal. Different kinds of electrodes are available; the glass membrane electrode is the most commonly used. This generates a potential related to pH value. The sensors based on ion-sensitive field effect transistors (ISFET) represent an alternative to the glass electrodes. They allow obtaining small and inexpensive pH sensors [SM16]. Optical methods are based on organic dye molecules with pH-dependent absorption spectra. In these systems, the colour of the organic dye changes on the basis of the pH value [AOKK08]. The accuracy of the pH measurement strongly depends on the spectral properties of the organic dye and it is usually higher than that achieved with the electrochemical methods. Test strips are the most common optical-based pH indicators. They are formed by a mixture of absorption indicator dyes that cover the pH range of interest, and they have a typical accuracy of 1.0 or 0.5 pH units. The main advantages of the test strips are the affordability and the rapidity of the measurement, while the disadvantages are the limited accuracy compared to the electrochemical instruments and the difficult of reading the result comparing the colour of the test strip and the reference, especially when the liquid under test can affect the colour of the test strip. To overcome these problems, several papers have proposed systems based on image colour detection to read the pH level of the

test strips [DSPN15, LVCL11, FAPK15, WLL$^+$18].

4.1.1 Beer Colour

The beer colour is strongly related to the beer style. It depends on the quantity of the several kinds of malts used in the recipe and the mashing process. Malt usually gives a pale colour to the beer. In order to obtain a darker colour, a quantity of caramelized and/or roasted malt has to be added to the recipe, in a suitable quantity. Brewers make the beer recipes according to the style and the physical and sensory characteristics they want to obtain. Then, they need to check the properties of the final product in order to verify the correctness of the recipe and the production process.
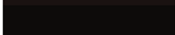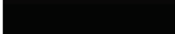

Figure 4.1: An example of the Lovibond Comparator.

Brewers use many technical methods to distinguish different beer colours and their intensities; one of the first methods was a colour scale developed by *Joseph Lovibond*. The Lovibond scale appeared for the first time towards the end of the nineteenth century when *Joseph W. Lovibond*, a British brewer, was the first to use some coloured slides to compare the colour of beer and classify it. Moreover, driven by the need to guarantee the quality of his products, he invented the first colourimeter, called Lovibond Comparator (Figure 4.1). It consisted of a metal wheel with scalloped edges, which housed sixteen coloured glasses, ranging from light amber to dark brown. A plate of transparent glass was placed in the wheel's centre, under which a small metal shelf protruded.

The master brewer would place a sample of beer in a clear glass container on the shelf of the instrument. By turning the wheel, the operator would match the colour of the sample with one of the coloured glasses. Each of the colours in the wheel represented a standard measurement called Lovibond Degrees. The colours were numbered and corresponded to different beers, from pale ale to imperial beer. Inherent errors in the visual comparison of colours due to the age of the standard slides used, the light used to illuminate the samples, the state of the observer, and various other issues made it difficult to achieve consistency between the outcomes of the different laboratories using the Lovibond scale.

In the middle of the twentieth century, to overcome the lack of objectivity of the Lovibond method, a method that leaves much room for human interpretation, the eye of the person looking at the slide, and therefore is also fallible or not accurate to the end, were introduced two new standards for the mea-

SRM	Beer Style	Beer colour	EBC
2	Pale lager, Witbier, Pilsener, Berliner Weisse		4
3	Maibock, Blonde Ale		6
4	Weissbier		8
6	American Pale Ale, India Pale Ale		12
8	Weissbier, Saison		16
10	English Bitter, ESB		20
13	Biere de Garde, Double IPA		26
17	Dark lager, Vienna lager, Marzen, Amber Ale		33
20	Brown Ale, Bock, Dunkel, Dunkelweizen		39
24	Irish Dry Stout, Doppelbock, Porter		47
29	Stout		57
35	Foreign Stout, Baltic Porter		69
40+	Imperial Stout		79

Figure 4.2: Standard Referenc Method (SRM) and European Beer Color (EBC) reference chart with beer style.

surement of colour: the **SRM** standard (Standard Reference Method) in the
United States and the **EBC** (European Beer Color) in Europe. The SRM and
EBC are based on the use of a spectrophotometer; their scales basically indi-
cate how much light, with its intensity adjusted to 430 nm, can pass through
one centimetre of beer inside a photometer. Beer colours measured in SRM
degrees and Lovibond degrees were similar when spectroscopy was adopted as
the reference method Figure 4.2. However, modern analytical methods show
that SRM and Lovibond diverge in the case of darker colours.

Determining the SRM value involves measuring the attenuation of light at
a particular wavelength as it passes through a test tube containing beer. The
attenuation is expressed by absorbance, which is scaled by a constant. The
measurement method for the SRM and EBC standards is identical. W hat
differentiates the two standards is a multiplicative constant used for scaling
the absorbance: the values of the EBC scale are approximately twice those of
the SRM scale. It is possible to determine the relationship between the scales
to convert the results:

$$SRM \rightarrow Lovibond \quad \Longleftrightarrow \quad {}^{\circ}L = \frac{(SRM + 0.6)}{1.3546}, \tag{4.1}$$

$$Lovibond \rightarrow SRM \quad \Longleftrightarrow \quad SRM = (1.35 * {}^{\circ}L) – 0.76, \tag{4.2}$$

$$EBC \rightarrow SRM \quad \Longleftrightarrow \quad SRM = EBC * 0.508, \tag{4.3}$$

$$SRM \rightarrow EBC \quad \Longleftrightarrow \quad EBC = SRM * 1.97. \tag{4.4}$$

Nowadays the standard method for the determination of the beer colour is
the spectrophotometry, which has the advantage of being independent from the
light condition that can alter the colour perception. The drawback is that the
spectrophotometer is a quite expensive instrument. An alternative method,
mainly used in the past, is the visual comparison of a beer sample with colour
references, but it strongly depends on the operator, the lighting condition
during the comparison and the quantity of beer used as sample. Several factors
make colour an important quality parameter in the beer production. Like
other visual appearance characteristics, it affects the quality perception and

the taste expectation in the consumers. Moreover, it provides direct and indirect indications of quality to the producers [Fra95, CMWS17].

4.2   Devices for Colour Measurement

The spectrophotometric method is based on the Beer-Lambert law relating the radiant power of a light source incident on an absorbing medium to the length of the path and the concentration species in that medium. The transmittance (T) of the absorbing medium can be defined as:

$$T = \frac{P}{P_0} \tag{4.5}$$

where P_0 is the radiant power of the incident source and P is the power that pass through the absorbing medium. The absorbance (A) is defined as:

$$A = -\log_1 0T = a(\lambda) \cdot b \cdot c \tag{4.6}$$

where a is the absorptivity, or extinction coefficient, which is wavelength-dependent, b is the path length and c is the concentration of the absorbing species [Swi62, CWL$^+$17].

The spectrophotometric method can be applied to all types of beer, the wort and the coloured malt products. It consists of the measurement of the absorbance of the liquid under test at a wavelength of $430\,\mathrm{nm}$ in a $10\,\mathrm{mm}$ cuvette by means of a spectrophotometer, and then the colour is obtained in the European Brewing Convention (EBC) units or in the Standard Reference Method (SRM) units, respectively as:

$$\text{EBC colour} = 25 \cdot A \cdot f \tag{4.7}$$

$$\text{SRM colour} = 12.7 \cdot A \cdot f \tag{4.8}$$

where f is the dilution factor that is used in order to obtain a value of absorbance at $430\,\mathrm{nm}$ within the linearity of the spectrophotometer. Besides
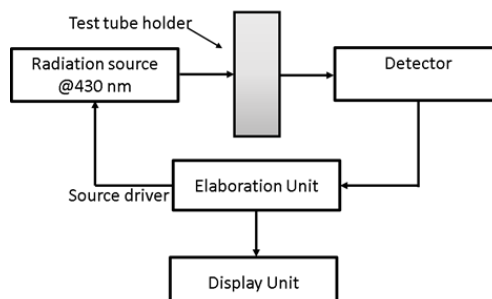
Figure 4.3: Block diagram of the proposed colour measurement system.

the dilution, the measurement procedure requires also the decarbonation of the sample under test, consisting in the removal of the carbon dioxide (CO_2) contained into the sample. This is because the gas bubbles can affect the accuracy of the measurement. The decarbonation can be obtained using several techniques, like manual or automating shaking, filtration, magnetic stirring.

The low-cost system for the colour measurement proposed in this work is based on the spectrophotometric method. It is composed by the following components (Figure 4.3):

- Radiation source, a LED at 430 nm;

- Detector consisting in a photo-detector with center wavelength of 900 nm;

- Elaboration Unit with display;

- Test tube holder where the LED and the detector are dipped.

The system implements the spectrophotometric method exploiting a radiation source at 430 nm wavelength. The absorbance depends on the colour of the beer sample placed in the test tube between the radiant source and the detector. Keeping constant the emitted light intensity from the radiation source the photocurrent generated by the detector is measured by means of a transimpedance amplifier and then fed into the ADC of the elaboration unit.

The range of variation of the absorbance between the pale and the darkest beers is very high. For this reason, in commercial spectrophotometers, a

dilution factor is used in order to obtain a value in the linear range of the instrument. In the proposed system, two different ranges of radiation intensity have been used for lith and dark beers: a lower value for the first and an higher one for the latter. In this way, it is possible to measure the colour of all kinds of beer avoiding sample dilution. In addition, the system is able to detect if the carbon dioxide has been effectively removed from the sample before the test. This is obtained measuring the time variation of the radiation at the detector side. The presence of residual CO_2 inside the beer sample causes a variation of the absorbed radiation and then a variation of the detected radiation that can be measured by the elaboration unit. In this case, a warning message is sent to the display unit instead of performing the colour measurement.

The sensing head of the proposed system is based on a couple LED photoreceiver. For the LED a L-53MBC low power and low cost device has been used, it is made with GaN on a SiC substrate. This device comes in a standard 5 mm package and it has a peak radiation wavelength at about 430 nm with a large spread but with a narrow radiation beam of about ±10°, as can be seen in Figure 4.4.

The device chosen as photoreceiver is a silicon PIN photodiode: BPV10. As the LED, it presents in a classical 5 mm clear plastic package, and has a spectral sensitivity varying from 380 nm to 1100 nm. The receiving angle is of about ±20°.

Both the devices were mounted in a fixed position on the holding tube, a device designed to hold both the devices and the glass tube in a fixed position. In Figure 4.5 the drawings of the holder are reported. The receiver and the emitter are inserted in the lateral holes at an height that is approximatively the half of the sample tube.

The sensing device and the illumination are axially aligned by design, instead no care is placed in the radial alignment due to the intrinsic symmetry of the devices packages. The tube glass containing the sample beer, slides in the holder from the top. In order to be able to remove the sample from the
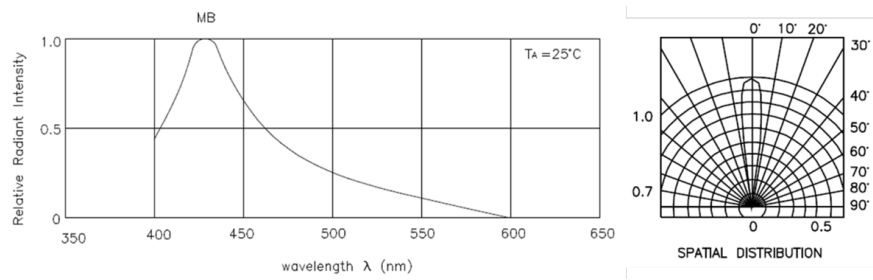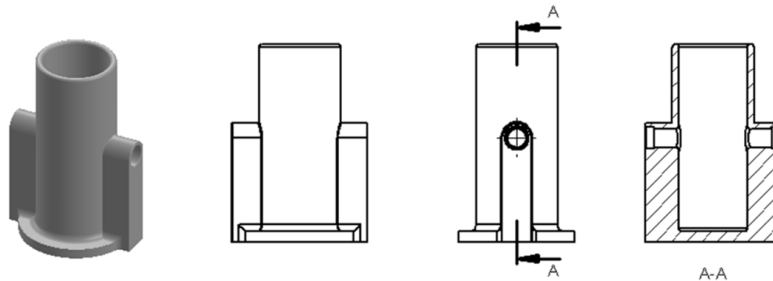
(a) Relative radiant Intensity and spatial distribution of the L-53MBC. Data taken from Kingbright specsheet no. DSAA5610 rev. 4
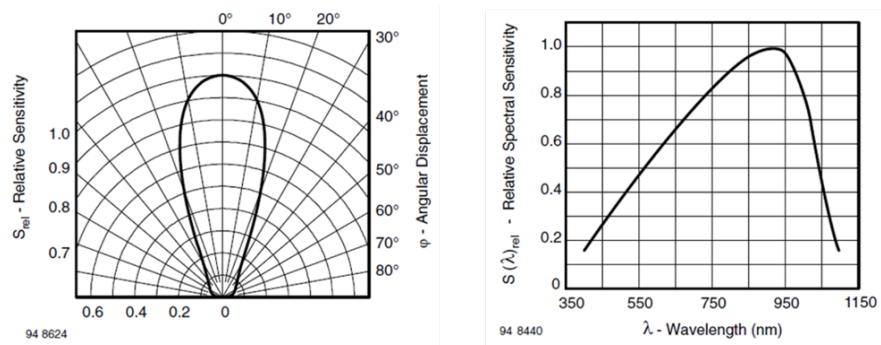
(b) Spectral sensitivity and relative spatial sensitivity of the BPV10. Data taken from VISHAY document no. 81502 rev. 1.9

Figure 4.4: Spectral intensity for the L-53MBC and BPV10 devices.

Figure 4.5: Holding tube design. From the left to right: a 3D rendering, front view, lateral view and a section showing the holes for the photoreceiver and the LED.

holding tube it has a diameter larger than the maximum diameter of the glass tube due to the production tolerances. The holding tube was made of black PLA polymer to shield the sensing head from the external lighting conditions, moreover a top cup was designed and adopted to further more prevent the ambient light to alter the measure.

Due to the nature of the radiation intensity of the LED proportional to the current flowing to its terminal the device is driven with a constant current circuit. It uses a general purpose low cost MOSFET, a $100\,\Omega$ shunt resistor and an operational amplifier to regulate the current flowing in the LED connected between the positive power supply rail and the MOSFET drain. The shunt and the operational amplifier form a feedback loop, keeping the voltage on the resistor at a target value imposed by a variable reference driven by the control unit, giving the possibility to change the illumination factor within the firmware, controlling a Pulse Width Modulation (PWM) duty cycle. The waveform at logic levels ($V_{\text{low}} = 0\,\text{V}$ and $V_{\text{high}} = 5\,\text{V}$) with a frequency of $10\,\text{kHz}$ is fed into a low pass filter that removes the high frequency harmonics to obtain a variable DC value proportional to the duty cycle. In this way the illumination intensity is directly controlled but its value still depends on the manufacturing tolerances of the LED device.

The diode used as the photoreceiver is reversely polarized to obtain the maximum gain in terms of sensitivity. A trains-impedance amplifier (TIA) has been used to convert the photogenerated current of the device into a voltage that is fed to the Analog to Digital Converter (ADC) of the microcontroller unit. In the feedback loop of the amplifier a resistor of $1\,M\Omega$ with a $22\,pF$ capacitor in parallel is used to set the transimpedance gain, to have the maximum amplification possible and span over the entire range of the microcontroller ADC. The parallel capacitor limits the bandwidth of the circuits but does not present any limitation in the measurement due to the quasi static nature of the involved phenomena. Furthermore the ADC values are sampled and averaged prior to be used in the measurement loop.

The elaboration unit is a microcontroller from Microchip Technology the ATmega328, it is based on a 8 bit advanced RISC architecture with a hardware multiplier. It features 32 Kbytes of flash program memory, 2 Kbytes of static RAM and 1 Kbytes of EEPROM where the calibration coefficients are stored. The microcontroller has a 10 bit resolution analog to digital converter, that has been used to acquire data from the TIA circuit, a simplified circuit diagram for this amplifier is reported in Figure 4.6. The microcontroller communicates with an OLED display via a Serial Peripheral Interface (SPI).
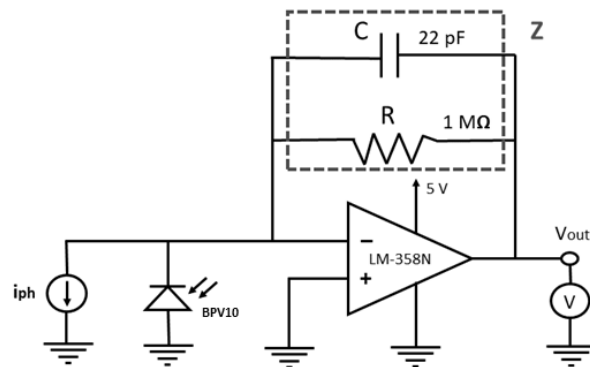
Figure 4.6: Simplified Trans Impedance Amplifier (TIA) circuit diagram.

The circuit in Figure 4.6 adapts the photocurrent signal, transforming it

in a voltage that can be measured by the analog to digital converter of the microcontroller. The photodiode can be modelled as a current generator, in the circuit I_{ph} [RCJ10]. The current I_{ph} goes through $Z(j\omega)$ impedance and generates a current at the circuit output V_{out}, given by:

$$V_{out} = I_{ph} * Z(j\omega) = \frac{I_{ph}R}{1 + j\omega RC},$$
(4.9)

with a voltage gain of:

$$G(j\omega) = \frac{V_{out}}{T_{ph}} = \frac{R}{1 + j\omega RC}.$$
(4.10)

The implemented firmware has the role to manage the sensing device and the illumination, carry out the measurement and show the user the properly converted result or any warning message. It is able to distinguish between dark and light beers using a preliminary measure made with the high illumination intensity range. When the measured value exceeds a fixed threshold value the system resembles a light beer and changes the LED intensity accordingly. When the measurements are in the correct range for both types of beers the algorithm proceeds with the acquisition of data samples. The variance of the samples in a fixed period of time is controlled to identify the presence of bubbles in the sample beer, in this case the user is warned with a message on the display. In other cases the microcontroller provides a converted measure to the end user on the same interface. Do to the non linear relation between the EBC value and the measured photo current a look up table (LUT) has been implemented to convert the acquired voltages samples into a EBC value.

4.2.1   pH Strip Measurement Device

he main issue working with beer is represented by the different colours of the samples that can affect the color detection of the pH strips. In addition, automatic colour detection is influenced by the presence of shades and light conditions. A correct pH range has to be guaranteed in each stage of the beer production since it influences the efficiency of enzymes [Meu09]. For this
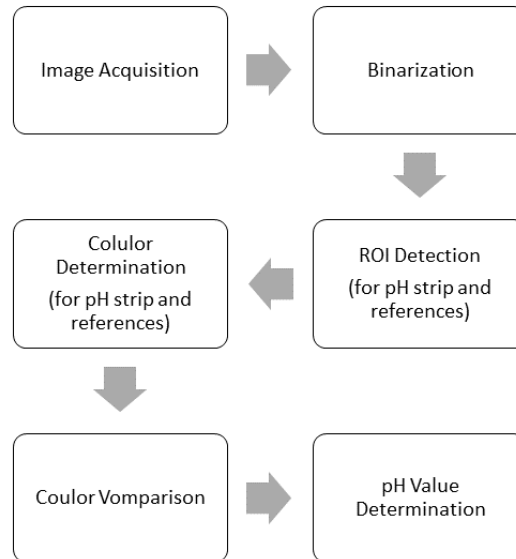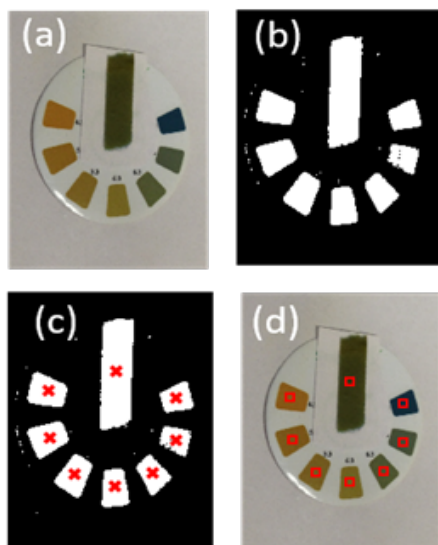
Figure 4.7: Image Processing Algorithm for pH value extraction.

reason, pH measurement is needed both for the hot water used in the process and in the mashing stages. A pH drop occurs during beer fermentation, typically from 5.2-5.6 to 4.3-4.6 [Meu09], then, pH measurement allows monitoring the fermentation process. Considering the different processing in beer production, the pH measurement is made on substances (water, wort, beer) that are neutral or acidic.

It is possible to obtain a pH reader based on an image processing algorithm that allows determining the pH level through the elaboration of the picture of a test strip taken with a smartphone camera. The picture containing the pH strip can be analysed determining the value of the pH level. The image processing algorithm includes a number of steps, as depicted in Figure 4.7. The first steps allow obtaining the regions of interest (ROI) related to the pH strip and the color references. They include the image binarization that allows detecting the regions containing the pH strip and the colour references, the centroid calculation of the detected regions and the ROI selection around

Figure 4.8: Different stages of the image processing algorithm applied on a test strip.

the centroids. Then, the colour of the ROI related to the pH strip and the references is determined. Finally, the colour of the pH strip is compared with the colour of the references and the pH value is determined. In order to establish the best parameter to discriminate among the colours of the pH strips to determine the pH level. In Figure 4.8 four different images are reported, each of them represents a single step of the processing algorithm.

4.3 Experimental Results

The results presented focus on the EBC range up to 35, which corresponds to the colour from pale to amber. The tests have been carried out on seven commercial beers with the colour in the selected range. The colour in EBC unit was determined according to the standard spectrophotometric method using a reference instrument: *PerkinElmer Lambda 800* spectrophotometer [Per]. Then, the same beer samples were tested using the proposed system,

considering both the photodiodes previously described and comparing the results.

The beer samples were numbered in ascending order of EBC colour. According to the standard spectrophotometric method, different dilution factors have been employed for the different samples in order to stay in the linear range of the spectrophotometer measuring the absorbance at 430 nm. For each sample, two measures were done and the mean value has been used as absorbance value to determine the EBC colour according to [Con07]. The results related to the reference method are reported in Table 4.1.

Sample	Dilution Factor	Absorbance at 430 nm	EBC
1	5	0.0676	8.5
2	10	0.0347	8.7
3	10	0.0413	10.3
4	10	0.0546	13.6
5	10	0.0659	16.5
6	10	0.0853	21.1
7	35	0.0392	34.3

Table 4.1: EBC colour measured using the reference spectrophotometric method.

## 4.3.1 Proposed System with 430 nm Photodiode

The beer samples have been tested with the proposed system implemented with the diode at 430 nm as radiation source and the photodiode at 430 nm as detector. For each sample, the TIA output voltage was measured, considering the mean value over 10 measures. This voltage represents the quantity of source radiation at 430 nm that is not absorbed by the sample and is received by the detector.

As expected, the detector voltage decreases when the colour of the beer becomes darker. A calibration curve was obtained considering the relation be-

Sample	V_{DETECTOR}	Measured EBC colour	Error
1	3.19 V	8.9	0.4
2	2.91 V	9.5	0.8
3	2.46 V	10.8	0.5
4	2.20 V	11.8	-1.9
5	1.55 V	15.2	-1.2
6	1.01 V	20.9	-0.1
7	0.49 V	36.2	2.0

Table 4.2: Mean value of the voltage of the detector (TIA output), measured EBC colour and error.

tween the detector voltage and the EBC colour (Figure 4.9). A power regression was chosen as calibration curve, obtaining a coefficient of determination (R_2) of 0.9715
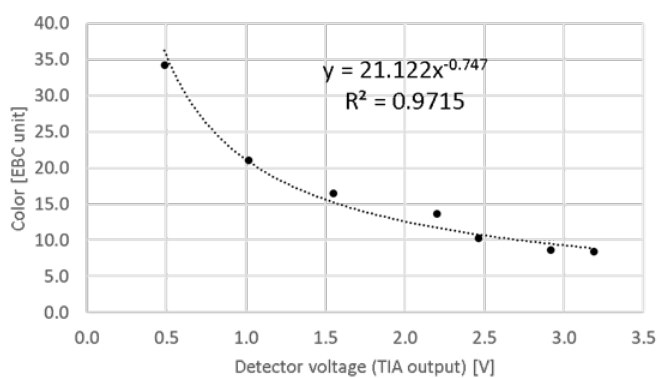
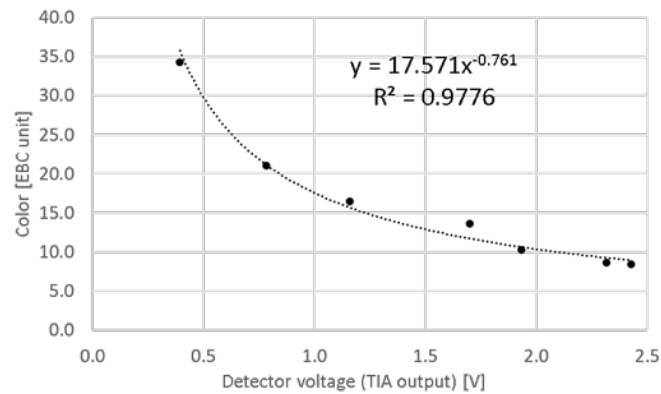**Figure 4.9:** Relation between the detector voltage and the EBC colour and regression curve.

Using the calibration curve the EBC colour of the samples under test, and the error respect to the reference values, have been determined (Table 4.2).

Sample	V_{DETECTOR}	Measured EBC colour	Error
1	2.43 V	9.0	0.5
2	2.32 V	9.3	0.6
3	1.93 V	10.6	0.3
4	1.70 V	11.7	-1.9
5	1.16 V	15.7	-0.8
6	0.78 V	21.1	0.1
7	0.39 V	35.7	1.4

Table 4.3: Mean value of the voltage of the detector (TIA output), measured EBC colour and error fr the low cost device.

4.3.2 Proposed System with Low-Cost Photodiode

The system implemented with the low-cost photodiode as detector was tested, using the same method employed for the system with the more expensive photodiode at 430 nm, in order to compare the performances. Figure 4.10 shows the obtained calibration curve, while the measured EBC colour and the error respect to the reference values are shown in Table 4.3.

Figure 4.10: Relation between the detector voltage and the EBC colour and regression curve for the low cost device.

Sample	Reference Device	Device 2	Device 3	Device 4
1	2.43 V	2.45 V	2.28 V	2.07 V
2	2.32 V	2.35 V	2.18 V	1.97 V
3	1.93 V	1.94 V	1.82 V	1.66 V
4	1.70 V	1.71 V	1.61 V	1.45 V
5	1.16 V	1.18 V	1.10 V	0.98 V
6	0.78 V	0.79 V	0.74 V	0.68 V
7	0.39 V	0.38 V	0.37 V	0.34 V

Table 4.4: Mean value of the voltage of the detector (TIA output) of the four tested devices.

As for the previous implementation, a power regression was chosen as calibration curve, and the results of the two systems are comparable. For this reason, the system implemented with the general purpose photodiode was preferred in order to decrease the cost.

Considering the parameter variation in different components respect to the nominal values, an analysis of the effect of these variation on the performances of the system was carried out. In particular, three different devices were used, employing three different diodes and photodiodes with the same model and manufacturer of the first tested device, which was considered as reference device. Table 4.4 shows the voltage of the detector related to the four devices.

As it can be seen in Table 4.4, the devices exhibit different voltages of the detector for the same beer sample, due to the different characteristics of the diodes and photodiodes employed. For this reason, it is not possible to use the same calibration curve for several devices. To overcome this problem, a pre-calibration procedure is proposed. First, the relation between the voltage of the detector of the new devices and the reference device (device 1) was considered (Figure 4.11).

As it can be seen in Figure 4.11, a linear relation has been obtained, with a coefficient of determination greater than 0.99. The regression curves related
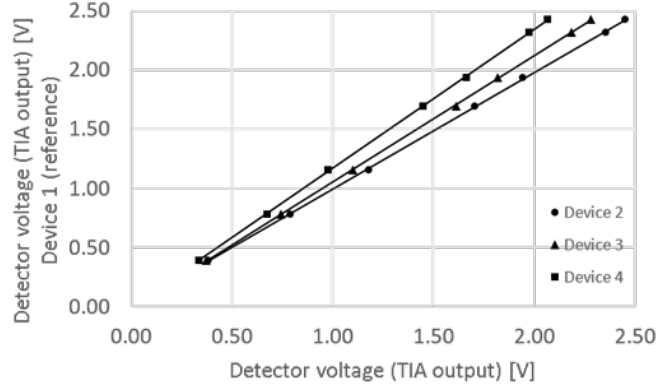
Figure 4.11: Relation between the detector voltage of the different devices respect to the reference device (device 1).

to the three devices are in the form:

$$V_D = k_n V_{Dn} \quad with \ n = 2, 3, 4 \tag{4.11}$$

The regression coefficients obtained for the three devices under test are:

$$k_2 = 0.985, \quad k_3 = 1.064, \quad k_4 = 1.172 \tag{4.12}$$

The equation (4.11) was used to correct the calibration curve of the reference device (4.13).

$$EBC \quad colour = 17.571 V_D^{-0.761} = 17.571(k_n V_{Dn})^{0.761} \quad with n = 2, 3, 4 \tag{4.13}$$

Finally, the results of the EBC colour calculation for the three devices using the calibration curve of the reference device and the corrected curve with the proposed pre-calibration method are shown in Table 4.5.

| Sample | Device 2 | | | | Device 3 | | | | Device 4 | | | |
| | With Pre-calibration | | Without Pre-calibration | | With Pre-calibration | | Without Pre-calibration | | With Pre-calibration | | Without Pre-calibration | |
	EBC	Err.	EBC	Err.	EBC	Err.	EBC	Err.	EBC	Err.	EBC	Err.
1	9.1	0.6	8.9	0.4	9.0	0.5	9.4	0.9	9.0	0.5	10.1	1.7
2	9.4	0.7	9.2	0.5	9.3	0.6	9.7	1.0	9.3	0.6	10.5	1.8
3	10.8	0.5	10.6	0.3	10.7	0.3	11.1	0.8	10.6	0.3	11.9	1.6
4	11.9	-1.7	11.7	-1.9	11.7	-2.0	12.2	-1.4	11.7	-1.9	13.2	-0.4
5	15.7	-0.7	15.5	-0.9	15.7	-0.8	16.4	-0.1	15.9	-0.6	17.9	1.4
6	21.1	0.1	21.0	-0.1	21.1	0.0	22.0	0.9	21.0	-0.1	23.7	2.6
7	36.4	2.2	36.6	2.3	35.8	1.6	37.4	3.1	35.8	1.5	40.4	6.1

Table 4.5: Comparison of the EBC colour determined with and without the pre-calibration method.

4.3.3   pH Strip Image Processing

preliminary tests have been carried out on pH test strips produced by Simple
Health with a range from 4.5 to 7.5 pH units with a resolution of 0.5 unit.
The colour of the test strip changes when dipped in a liquid. The pH value is
determined comparing the colour of the strip with that of the seven references,
each one associated to a pH level Figure 4.12.

Figure 4.12: On the left a pH test strip, and on the right the colour references
with associated pH level.

The tests were divided in two phases: first, an analysis of the colour of the
pH references was carried out comparing the relation between the components
of several colour spaces with the pH level, to find the best parameter that
allows to determine the colour of the different references. Then, the selected
parameter was used in the processing algorithm, verifying the performances
using beer wort samples with different pH values.

The analysis of the colour of the pH references was made comparing the
relation between the components of several colour spaces and the pH level,
considering different light conditions. A colour space is a mathematical model
that represents a colour as a combination of different components. In this
work, RGB, HSV and LAB colour spaces have been taken into account. RGB
considers a colour as the composition of the red (R), green (G) and blue (B)
components. HSV is an alternative colour representation based on hue (H),
saturation (S) and value (V). LAB was defined by the Commission Interna-
tionale de l'Eclairage (CIE). It uses three coordinates representing the lightness

(L), the red/green balance (A) and the green/blue balance (B) [SCB87, JG78].
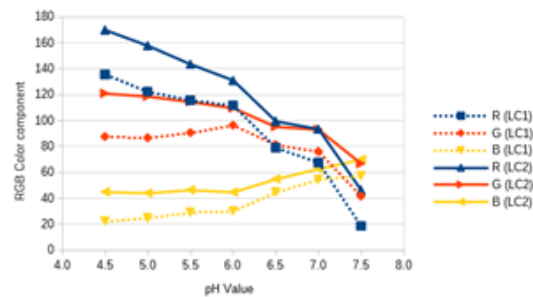
(a) Relation between RGB components and pH references for low level lighting (LC1) and high level lighting (LC2).
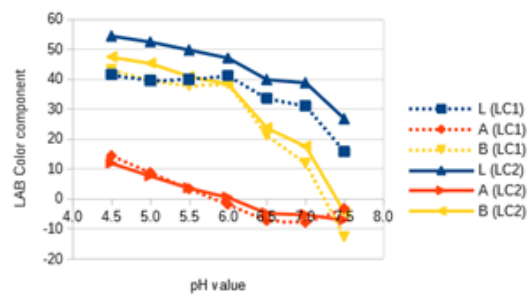
(b) Relation between LAB components and pH references for low level lighting (LC1) and high level lighting (LC2).
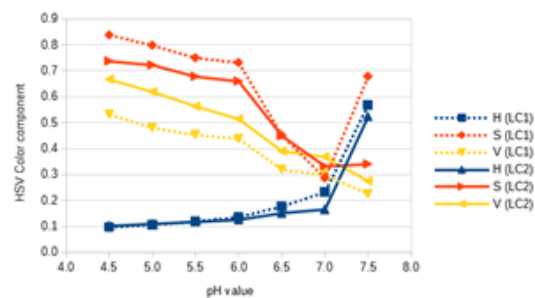
(c) Relation between HSV components and pH references for low level lighting (LC1) and high level lighting (LC2).

Figure 4.13: Relations betweens the three different colour spaces (RGB, LAB and HSV) and the pH references values for different lighting conditions.

The relation between the components of these colour spaces and the pH level of the references is shown in Figure 4.13, considering two light conditions, low level (LC1) and high level (LC2). The hue (H) component of the HSV colour space exhibited the smallest variation with a change of light condition and an increasing value when the pH raises. For these reasons, it has been used as colour determination parameter in the processing algorithm.

The processing algorithm has been tested with six samples of beer wort with different pH value. The actual pH value was measured using a digital pH-meter. For each test, ten samples of beer wort were used. For each sample, a picture containing the pH strip and the colour references was taken, then the hue was calculated as mean value related to the pixels in the ROI. After that, the pH was determined comparing the hue (H) of the strip and the color references, considering the linear interpolation between the H values related to two adjacent color references.

The pH value has been calculated by means of the following equation:

$$pH_{\text{strip}} = pH_{\text{ref 1}} + (H_{\text{strip}} - H_{\text{ref 1}}) \frac{pH_{\text{ref 2}} - pH_{\text{ref 1}}}{H_{\text{ref 2}} - H_{\text{ref 1}}}, \qquad (4.14)$$

where H_{strip} is the hue of the strip, $H_{\text{ref 1}}$ and $H_{\text{ref 2}}$ are the hue of the colour references with $H_{\text{ref 1}} < H_{\text{strip}} < H_{\text{ref 2}}$, $pH_{\text{ref 1}}$ and $pH_{\text{ref 2}}$ are the values of pH associated to the colour references with $H_{\text{ref 1}}$ and $H_{\text{ref 2}}$ value.

Some results are shown in Table ??. As it can be seen, the interpolation of the hue values using the linear interpolation allows to improve the pH strip accuracy. The preliminary test, carried out on beer samples, highlighted that it is possible obtaining the pH value with an accuracy lower than nominal value of the pH test strips.

pH value	Measured pH	
	Mean	Std. Dev.
4.78	4.84	0.09
5.64	5.86	0.11
6.26	6.23	0.11
6.46	6.31	0.18
6.70	6.59	0.25
7.31	7.12	0.09

Table 4.6: pH value calculated using the proposed algorithm.

References

[AOKK08]   Hiroaki Aizawa, Kenichi Okubo, Tooru Katsumata, and Shuji Komuro. Optical ph measurement method using organic dye film. In *2008 SICE Annual Conference*, pages 2192–2195, 2008.

[Bee]   European beer trends, statistics report, edition 2019, brussels. `https://brewersofeurope.org/uploads/mycms-files/documents/publications/2019/european-beer-trends-2019-web.pdf`.

[CMWS17]   Felipe Reinoso Carvalho, Pieter Moors, Johan Wagemans, and Charles Spence. The influence of color on the consumer's experience of beer. *Frontiers in Psychology*, 8, 2017.

[Con07]   European Brewery Convention. *Analytica - EBC*. Nuurnberg: Hans Carl, Fachverlag, 2007.

[CRS09]   Anthony J. Cutaia, Anna-Jean Reid, and R. Alex Speers. Examination of the relationships between original, real and apparent extracts, and alcohol in pilot plant and commercially produced beers. *Journal of the Institute of Brewing*, 115(4):318–327, 2009.

[CWL+17]   Po-Jui Chen, Hsiao-Ting Wang, Lih-Yuan Lin, Ban-Dar Hsu, Da-Ren Liu, Chi-Hung Hwang, and Wen-Hong Wu. A practical portable photometer using leds as inspection light source. In *2017 IEEE International Instrumentation and Measurement Technology Conference (I2MTC)*, pages 1–6, 2017.

[DSPN15]   Sibasish Dutta, Dhrubajyoti Sarma, Arbind Patel, and Pabitra Nath. Dye-assisted ph sensing using a smartphone. *IEEE Photonics Technology Letters*, 27(22):2363–2366, 2015.

[FAPK15]   Altamash Fakki, Salahaldein Ahmed, Jongwon Park, and Chang-Soo Kim. Optical mouse as ph analyzer. In *2015 IEEE SENSORS*, pages 1–4, 2015.

[Fra95]   F.J. Francis. Quality as influenced by color. *Food Quality and Preference*, 6(3):149–155, 1995. The Definition and Measurement of Quality.

[GVMRM+11]   Mahdi Ghasemi-Varnamkhasti, Seyed Mohtasebi, María Rodríguez-Méndez, Jesús Lozano, Seyed Razavi, and Hojat Ahmadi. Potential application of electronic nose technology in brewery. *Trends in Food Science and Technology*, 22:165–174, 04 2011.

[JG78]   George H. Joblove and Donald Greenberg. Color spaces for computer graphics. In *Proceedings of the 5th Annual Conference on Computer Graphics and Interactive Techniques*, SIGGRAPH '78, page 20–25, New York, NY, USA, 1978. Association for Computing Machinery.

[LDR+15]   Loredana Liguori, Giovanni De Francesco, Paola Russo, Giuseppe Perretti, Donatella Albanese, and Marisa Di Matteo. Production and characterization of alcohol-free beer by membrane process. *Food and Bioproducts Processing*, 94:158–168, 2015.

[LMM+19]   Jasmina Lukinac, Kristina Mastanjević, Krešimir Mastanjević, Gjore Nakov, and Marko Jukić. Computer vision method in beer quality evaluation—a review. *Beverages*, 5(2), 2019.

[LVCL11]   B Loh, Khue Vuong, Syin Chan, and C Lau. Automated mobile ph reader on a camera phone. *IAENG International Journal of Computer Science*, 38, 08 2011.

[Meu09] Franz G. Meussdoerffer. *A Comprehensive History of Beer Brewing*, chapter 1, pages 1–42. John Wiley and Sons, Ltd, 2009.

[oAB09] Handbook of Alcoholic Beverages. *Beer: A Quality Perspective.* Charles W. Bamforth, 2009.

[Per] PerkinElmer Instruments LLC. *Lambda 800/900 User's Guide.* Last accessed 02 February 2022.

[RCJ10] Travis N. Blalock Richard C. Jaeger. *Microelectronic circuit design.* McGraw-Hill Science/Engineering/Math, 4 edition, 2010.

[SCB87] Michael W. Schwarz, William B. Cowan, and John C. Beatty. An experimental comparison of rgb, yiq, lab, hsv, and opponent color models. *ACM Trans. Graph.*, 6(2):123–158, apr 1987.

[SLA17] José Pedro Santos, Jesús Lozano, and Manuel Aleixandre. Electronic noses applications in beer technology. In Makoto Kanauchi, editor, *Brewing Technology*, chapter 9. IntechOpen, Rijeka, 2017.

[SM16] Mst Shamim Ara Shawkat and Nicole McFarlane. A single-chip isfet based ph sensor. In *2016 IEEE SENSORS*, pages 1–3, 2016.

[Swi62] D. F. Swinehart. The beer-lambert law. *Journal of Chemical Education*, 39(7):333, 1962.

[WLL$^+$18] Ying Wang, Yue Liu, Wen Liu, Wenhao Tang, Li Shen, Zhilin Li, and Meikun Fan. Quantification of combined color and shade changes in colorimetry and image analysis: water ph

measurement as an example. *Anal. Methods*, 10:3059–3065, 2018.

[YJK05]   Miao Yuqing, Chen Jianrong, and Fang Keming. New technology for the detection of ph. *Journal of Biochemical and Biophysical Methods*, 63(1):1–9, 2005.

[ZSI+15] Z. Zulkarnay, S. Shazwani, B. Ibrahim, A. J. Jurimah, A. R. Ruzairi, and S. Zaridah. An overview on ph measurement technique and application in biomedical and industrial process. In *2015 2nd International Conference on Biomedical Engineering (ICoBE)*, pages 1–6, 2015.

Conclusions

Machine vision systems have proven and demonstrate that they fully meet users' needs in various sectors. The typical industrial applications linked to the automation of any visual controls are now flanked by unconventional scenarios that make the use of artificial vision systems a powerful, robust and omnipresent tool even more.

The use of visual inspection and image processing in the industry about product or tool quality control are typical in machining in the mechanical and related industry: dimensional checks, integrity checks, checks for the presence of objects or defects or the monitoring of tools such as cutters and drill bits. The application presented relates to the estimation of the state of wear of the drill bits through the use of image processing techniques. The literature reports examples of this type of analysis applied to small diameter tools, PCB drilling, or tools of considerable size for machine tools and heavy machining. In both contexts, the proposed solutions often require complex alignment systems, both motorized and non-motorized, or use high-cost lighting techniques based on polarized light. The proposed solution solves these two problems with a low cost and easy to use the system while managing to guarantee acceptable results. Using the computational imaging technique, it was possible to exploit an illuminator that did not require polarized light. The analysis of the images of the tip was found to be helpful in defining the state of life of the tip, and it was possible, by analyzing different tips in progressive aging conditions, to extract a model that generalizes the state of wear of the tip. The parameters extracted from the profile, average height, integral and devi-

ation, represent a good indicator for the quality of the drill and allow even an inexperienced operator to recognize and distinguish the drills that can be used for the drilling process. The vision system applied to the tip, instead of the hole itself, as it often happens in the industry, also allows to avoid costly repairs due to the reworking of products caused by an incorrect tolerance due to the drilling process.

Another alternative use of artificial vision techniques can be seen in analysing drinking water leaks, a vital problem already dealt with different ways. Current techniques for identifying water leaks are not based on the use of vision systems except in rare cases. One of them is robotic piping inspection, which is not always applicable, intrusive and expensive. The most used methods inspect the entire pipe network through vibration analysis or field inspections to identify the leak's location with a specific resolution, strictly depending on the technique used. The solution proposed in Chapter 3 concerns the identification of leaks at home using image analysis on standard analog meters with both digits and needles. The results obtained using the correlation technique on consecutive images allow discriminating the presence of water leaks from the ordinary conditions of use of the system for domestic applications. Compared with the other techniques proposed and already in use, this has the advantage of being permanently applicable at home, ensuring constant monitoring and a very high resolution on the localization of leaks. In this case, image processing, assisted by the availability of low-cost and high-performance acquisition and processing devices, generates a valuable and unconventional tool for a widespread problem.

The latest alternative use of vision techniques is applied to the growing microbrewery market. Computer Vision was already been successfully applied in the past to determine attributes related to both beer and its quality. The problem faced is the analysis of the beer colour, a fundamental indicator of product quality. Meanwhile, large industrial productions are controlled with expensive and difficult to use devices such as spectrometers; this does not

apply to microbrewery, where the costs need to be kept down. The alternative technique to using the spectrometer is an inspection by comparison entrusted to an expert operator, a technique that does not ensure a sufficient degree of reproducibility. In this last case, image analysis is reduced to analysing a specific spectrum of visible light captured through a single photo diode. From the analysis carried out with various devices, it was possible to successfully identify the colour of the beer using a very low-cost device by exploiting its optical properties and concentrating the range of analysis within the region of the spectrum of interest.

In conclusion, image analysis for unconventional applications in the industrial and non-industrial fields is currently a plausible alternative to conventional measurement techniques that can often be too expensive, time-consuming or even need highly qualified staff. Thanks to the progress of computer and electronic technologies, sensors, and research in computer vision and image processing and acquisition systems, it is now possible to make the most of devices with reduced dimensions and costs to analyse the quality of products, processes, or processes tools, which are often not identifiable with traditional methodologies.